



**HAL**  
open science

## Growing black holes and galaxies: black hole accretion versus star formation rate

Marta Volonteri, Pedro R. Capelo, Hagai Netzer, Jillian Bellovary, Massimo Dotti, Fabio Governato

► **To cite this version:**

Marta Volonteri, Pedro R. Capelo, Hagai Netzer, Jillian Bellovary, Massimo Dotti, et al.. Growing black holes and galaxies: black hole accretion versus star formation rate. Monthly Notices of the Royal Astronomical Society, 2015, 449, pp.1470-1485. 10.1093/mnras/stv387 . insu-03644954

**HAL Id: insu-03644954**

**<https://insu.hal.science/insu-03644954>**

Submitted on 26 Apr 2022

**HAL** is a multi-disciplinary open access archive for the deposit and dissemination of scientific research documents, whether they are published or not. The documents may come from teaching and research institutions in France or abroad, or from public or private research centers.

L'archive ouverte pluridisciplinaire **HAL**, est destinée au dépôt et à la diffusion de documents scientifiques de niveau recherche, publiés ou non, émanant des établissements d'enseignement et de recherche français ou étrangers, des laboratoires publics ou privés.

# Growing black holes and galaxies: black hole accretion versus star formation rate

Marta Volonteri,<sup>1★</sup> Pedro R. Capelo,<sup>2</sup> Hagai Netzer,<sup>3</sup> Jillian Bellovary,<sup>4</sup> Massimo Dotti<sup>5</sup> and Fabio Governato<sup>6</sup>

<sup>1</sup>*Institut d’Astrophysique de Paris, 98bis Boulevard Arago, F-75014 Paris, France*

<sup>2</sup>*Department of Astronomy, University of Michigan, Ann Arbor, MI 48109, USA*

<sup>3</sup>*School of Physics and Astronomy, The Sackler Faculty of Exact Sciences, Tel-Aviv University, Tel-Aviv 69978, Israel*

<sup>4</sup>*Department of Physics and Astronomy, Vanderbilt University, Nashville, TN 37235, USA*

<sup>5</sup>*Dipartimento di Fisica G. Occhialini, Università degli Studi di Milano Bicocca, Piazza della Scienza 3, I-20126 Milano, Italy*

<sup>6</sup>*Department of Astronomy, University of Washington, Box 351580, Seattle, WA 98195, USA*

Accepted 2015 February 19. Received 2015 January 9; in original form 2014 October 16

## ABSTRACT

We present a new suite of hydrodynamical simulations and use it to study, in detail, black hole and galaxy properties. The high time, spatial and mass resolution, and realistic orbits and mass ratios, down to 1:6 and 1:10, enable us to meaningfully compare star formation rate (SFR) and BH accretion rate (BHAR) time-scales, temporal behaviour, and relative magnitude. We find that (i) BHAR and galaxy-wide SFR are typically temporally uncorrelated, and have different variability time-scales, except during the merger proper, lasting  $\sim 0.2\text{--}0.3$  Gyr. BHAR and nuclear ( $<100$  pc) SFR are better correlated, and their variability are similar. Averaging over time, the merger phase leads typically to an increase by a factor of a few in the BHAR/SFR ratio. (ii) BHAR and nuclear SFR are intrinsically proportional, but the correlation lessens if the long-term SFR is measured. (iii) Galaxies in the remnant phase are the ones most likely to be selected as systems dominated by an active galactic nucleus, because of the long time spent in this phase. (iv) The time-scale over which a given diagnostic probes the SFR has a profound impact on the recovered correlations with BHAR, and on the interpretation of observational data.

**Key words:** galaxies: active – galaxies: interactions – galaxies: nuclei.

## 1 INTRODUCTION

Several known scaling relationships between supermassive black holes (BHs) and large-scale properties of their host galaxies, such as mass, luminosity, and velocity dispersion, primarily of the bulge component, suggest a joint galaxy and BH cosmic evolution (Magorrian et al. 1998; Ferrarese & Merritt 2000; Marconi & Hunt 2003; Häring & Rix 2004; Gültekin et al. 2009; Kormendy & Ho 2013). In particular, the almost linear correlation between BH mass and bulge mass suggests parallel growth. More specifically, ‘for every  $\sim 1000$  units of star formation (SF) there is  $\sim 1\text{--}2$  units of BH accretion’ (Alexander & Hickox 2012). Several observational studies attempted to compare BH accretion rate (BHAR) and SF rates (SFRs) on galactic scale (e.g. Netzer et al. 2007; Wild et al. 2007; Lutz et al. 2008; Netzer 2009; Wild, Heckman & Charlot 2010; Rosario et al. 2012) and subgalactic scales ( $<1$  kpc; Diamond-Stanic & Rieke 2012). In general, such a comparison

shows a large scatter which is somewhat reduced when the SFR is measured over  $<1$  kpc scales, the region more easily influenced by the BH, and more directly identified with the bulge (although bulges can be significantly larger).

Taking a statistical approach, Heckman et al. (2004), Merloni, Rudnick & Di Matteo (2004), and Silverman et al. (2008, 2009) argued that the volume-averaged ratio of BHAR to SFR is about constant up to  $z \sim 3$ . Mullaney et al. (2012) and Chen et al. (2013) further suggested that the measured BHAR/SFR ratio may vary wildly, mostly because the time-variability of BH accretion is much faster than that of SF (see also Aird et al. 2012; Hickox et al. 2014). In this view, BHAR and SFR may appear uncorrelated in sources taken one by one, but once a large sample is averaged the underlying correlation emerges.

Theoretical models have investigated AGN activity and SF on different levels (Kauffmann & Haehnelt 2000; Hopkins et al. 2006; Blecha et al. 2011; Hayward et al. 2014). Di Matteo, Springel & Hernquist (2005) and Springel, Di Matteo & Hernquist (2005) suggested that galaxy mergers enhance both BH activity and SFR. Thacker et al. (2014) performed a series of simulations of

\* E-mail: [martav@iap.fr](mailto:martav@iap.fr)

equal-mass galaxy mergers to study the SFR-BHAR correlation. They found that the evolution of BHAR and SFR in a single merger is highly complex and that the volume-averaged correlation is only approximate. Johansson, Naab & Burkert (2009) perform merger simulations with mass ratio as low as 1:6, and find that the growth time of BH and stellar mass is strongly correlated with the mass ratio of the merger. Silk (2013) develops a feedback model that couples SFR and BHAR via outflow-induced pressure-enhanced SF. This model predicts that, on average, BHAR  $\sim 10^{-3}$  SFR, modulated by the radiative and mechanical efficiencies. Gabor & Bournaud (2013) focus, instead, on isolated high-redshift gas-rich galaxies. They found that a wide range of SFRs is possible if the BHAR is low, because such low rates are characterized by high variability driven by the structure of the interstellar medium and by AGN feedback. Neistein & Netzer (2014) developed a semi-analytic model where BHs grow only during SF bursts caused by galaxy mergers. They naturally explained the lack of correlation between SFR and BHAR at low AGN luminosities as the measured SFR in such phases is being polluted by secular SF that occurred before the burst and hence is unrelated to the AGN activity. High-luminosity AGN, on the other hand, are observed at times that are close to the peak of the BH accretion event. In this case, the measured SFR traces the merger-driven burst, concurrent with the merger-driven AGN activity.

Previous calculations of galaxy mergers with different mass ratios do not have the required spatial and time resolution to follow nuclear inflows and resolve the different time-scales involving BH accretion and SF. Improving these resolutions would allow us to address, at the same time, the question of whether the time-dependent BHAR washes out an underlying correlation with SFR, and whether merging galaxies behave differently from quiescent ones.

The calculations presented in this paper focus on (1) the temporal correlation between SFR and BHAR; (2) the time-variability of SFR and BHAR; (3) the relative growth of stellar mass and BH mass before, during and after a merger; and (4) the relative magnitude of SFR and BHAR through all the phases of the merger event. The purpose is to address the assembly of stellar and BH mass, and the establishment of scaling relations. We take both the theorists' view, asking if an underlying correlation between SFR and BHAR exists, and the observers' view, asking if a putative underlying correlation between SFR and BHAR can be measured. The simulations represent a major improvement in this direction. Our new suite of hydrodynamical simulations provides very high spatial and temporal resolution (gas mass of  $\sim 5 \times 10^3 M_{\odot}$ , softening length of 20 pc for gas and 5 pc for the BHs, BH properties output every 0.1 Myr), a large range of initial mass ratios (1:1 to 1:10), several orbital configurations, and various gas fractions. In particular, we keep our time, masses, and spatial resolution very high throughout the entire merger process and are able to evolve the galaxies for a long time before and after the merger proper. This means that we are capturing the properties of galaxies in quiescence (hereafter 'stochastic') phases and between the 'merger' and the re-establishment of quiescence (hereafter 'remnant' phase). The main limitation of our suite is that it does not allow us to simulate large galaxies. Each of our mergers requires  $\sim 10^7$  particles, and the entire suite required  $\sim 10^8$  particles. The total equivalent simulated time amounted to  $\sim 30$  Gyr of evolution.

The structure of the paper is as follows: In Section 2, we present the numerical set-up. In Section 3, we describe the general behaviour of a typical merger and in Section 4, we discuss the temporal correlation between SFR and BHAR, while in Section 5, we compare the time-variability of SFR and BHAR. In Section 6, we study the

**Table 1.** Parameters for our simulations.  $\theta_1$  and  $\theta_2$  are the angles between the spin axis and the total orbital angular momentum axis for each galaxy.  $q$  is the initial mass ratio between the merging galaxies.

| Name             | Mass ratio ( $q$ ) | $\theta_1$ | $\theta_2$ | Gas fraction |
|------------------|--------------------|------------|------------|--------------|
| m1.gf0.3.pro     | 1:1                | 0          | 0          | 0.3          |
| m2.gf0.3.pro     | 1:2                | 0          | 0          | 0.3          |
| m2.gf0.3.incl    | 1:2                | $\pi/4$    | 0          | 0.3          |
| m2.gf0.3.retprim | 1:2                | $\pi$      | 0          | 0.3          |
| m2.gf0.3.retsec  | 1:2                | 0          | $\pi$      | 0.3          |
| m2.gf0.6.pro     | 1:2                | 0          | 0          | 0.6          |
| m4.gf0.3.pro     | 1:4                | 0          | 0          | 0.3          |
| m4.gf0.3.incl    | 1:4                | $\pi/4$    | 0          | 0.3          |
| m6.gf0.3.pro     | 1:6                | 0          | 0          | 0.3          |
| m10.gf0.3.pro    | 1:10               | 0          | 0          | 0.3          |

relative growth of stellar mass and BH mass; and in Section 7, we explain the various BH and SF relationships extracted from the simulations. In Section 8, we compare the relationship between BH and SF to observations.

## 2 NUMERICAL SET-UP

The numerical set-up includes a suite of hydrodynamical simulations applied to mergers of disc galaxies with mass ratios of 1:1, 1:2, 1:4, 1:6, and 1:10. The chosen redshift,  $z = 3$ , corresponds to the peak of the cosmic merger rate. The calculations and main results are presented below and the appendix adds the necessary information about the dependences on the numerical resolution and the assumed strength of AGN feedback.

### 2.1 Orbital configuration

We chose an orbital configuration that matches those of the most common halo mergers in cosmological simulations of galaxy formation (Benson 2005), where almost half of all mergers have an eccentricity  $e$  between 0.9 and 1.1. Khochfar & Burkert (2006) find that 85 per cent of merging halo orbits have initial pericentre distances in excess of 10 per cent of the virial radius of  $G_1$  ( $G_1$  and  $G_2$  are the larger and smaller galaxies, respectively). Most simulations of galaxy mergers consider smaller pericentre distances, to save computational time, producing more direct collisions. Instead, we set the initial pericentre distance near 20 per cent of the virial radius of  $G_1$ , in order to be consistent with cosmological orbits. The initial separation between the galaxies is set near the sum of the two virial radii. We summarize the orbital configuration for each simulation in Table 1.

We vary the angle between each galaxy's angular momentum axis and the overall orbital angular momentum vector, given by  $\theta$  in Table 1. We consider coplanar, prograde–prograde mergers, in which  $\theta_1$  and  $\theta_2$ , the angles for  $G_1$  and  $G_2$ , respectively, are both zero. In our inclined mergers, we set  $\theta_1 = \pi/4$  and  $\theta_2 = 0$ . Lastly, we consider coplanar, retrograde mergers, in which one of the galaxies is anti-aligned with the overall orbital angular momentum axis. In the coplanar, retrograde–prograde merger,  $\theta_1 = \pi$  and  $\theta_2 = 0$ . In the coplanar, prograde–retrograde merger,  $\theta_1 = 0$  and  $\theta_2 = \pi$ .

### 2.2 Galaxies

All galaxies are composite systems of dark matter, gas, stars, and a central BH (described in the next section). See Table 2 for a complete list. Most of this description follows Springel & White

**Table 2.** Main galactic parameters at the beginning of the simulation. (1) Galaxy (primary – G1 or secondary – G2) and merger. (2) Virial mass. (3) Stellar bulge mass. (4) Stellar disc mass. (5) Gas disc mass. (6) Disc scale radius. (7) BH mass. (8) Dark matter particle mass. (9) Dark matter particle softening length. The disc mass is the sum of the stellar disc mass and the gas disc mass. The stellar bulge scale radius and the disc scale height are always equal to  $0.2 r_{\text{disc}}$  and  $0.1 r_{\text{disc}}$ , respectively. All other parameters are the same for all galaxies and all mergers: gas and stellar particle mass ( $4.6 \times 10^3$  and  $3.3 \times 10^3 M_{\odot}$ , respectively) and softening (20 and 10 pc, respectively); BH softening (5 pc); dark matter halo spin and concentration parameters ( $\lambda = 0.04$  and  $c = 3$ , respectively); and redshift ( $z = 3$ ).

| Galaxy (Merger)                 | $M_{\text{vir}}$<br>( $10^{11} M_{\odot}$ ) | $M_{\text{stell. bulge}}$<br>( $10^9 M_{\odot}$ ) | $M_{\text{stell. disc}}$<br>( $10^9 M_{\odot}$ ) | $M_{\text{gas. disc}}$<br>( $10^9 M_{\odot}$ ) | $r_{\text{disc}}$<br>(kpc) | $M_{\text{BH}}$<br>( $10^6 M_{\odot}$ ) | $M_{\text{DM part.}}$<br>( $10^5 M_{\odot}$ ) | $\epsilon_{\text{DM part.}}$<br>(pc) |
|---------------------------------|---|---|--|--|----------------------------|---|---|--------------------------------------|
| G1 [1:1, 1:2, 1:4 low-gas-frac] | 2.21  | 1.77  | 6.19   | 2.65   | 1.13                       | 3.53                                    | 1.1   | 30                                   |
| G1 [1:2 high-gas-frac]          | 2.21  | 1.77  | 3.54   | 5.30   | 1.13                       | 3.53                                    | 1.1   | 30                                   |
| G1 [1:6]                        | 2.21  | 1.77  | 6.19   | 2.65   | 1.13                       | 3.53                                    | 0.8   | 27                                   |
| G1 [1:10]                       | 2.21  | 1.77  | 6.19   | 2.65   | 1.13                       | 3.53                                    | 0.5   | 23                                   |
| G2 [1:2 low-gas-frac]           | 1.11  | 0.88  | 3.09   | 1.33   | 0.90                       | 1.77                                    | 1.1   | 30                                   |
| G2 [1:2 high-gas-frac]          | 1.11  | 0.88  | 1.77   | 2.65   | 0.90                       | 1.77                                    | 1.1   | 30                                   |
| G2 [1:4]                        | 0.55  | 0.44  | 1.55   | 0.66   | 0.71                       | 0.88                                    | 1.1   | 30                                   |
| G2 [1:6]                        | 0.37  | 0.30  | 1.03   | 0.44   | 0.62                       | 0.59                                    | 0.8   | 27                                   |
| G2 [1:10]                       | 0.22  | 0.18  | 0.62   | 0.27   | 0.52                       | 0.35                                    | 0.5   | 23                                   |

(1999) and Springel, Di Matteo & Hernquist (2005).<sup>3</sup> Most values in this section were chosen for consistency with previous work (Callegari et al. 2009, 2011; Van Wassenhove et al. 2012, 2014) and in Table 2, we report the complete list of their properties and those of their central BHs (described in the next section). The dark matter halo is described by a spherical Navarro–Frenk–White profile (Navarro, Frenk & White 1997) with spin parameter  $\lambda = 0.04$ . The dark matter halo concentration parameter is initialized to  $c = 3$ . The disc has an exponential density profile with total mass equal to 4 per cent of the virial mass of the galaxy. The disc scale radius  $r_{\text{disc}}$  is then determined by imposing conservation of specific angular momentum of the material that forms the disc, whereas the disc scale height  $z_{\text{disc}}$  is set to be 10 per cent of  $r_{\text{disc}}$ . The gas in the disc has a mass fraction  $f_{\text{gas}} = 0.3$  or  $0.6$ . The stellar bulge is described by a spherical Hernquist (1990) density profile with total mass equal to 0.8 per cent of the virial mass of the galaxy. In each merger,  $G_1$  has a virial mass of  $2.24 \times 10^{11} M_{\odot}$  (consistent with Adelberger et al. 2005), and, consequently, a bulge mass of  $1.77 \times 10^9 M_{\odot}$ , a disc mass of  $8.84 \times 10^9 M_{\odot}$ , and a disc scale radius of 1.13 kpc. The mass and all the other properties of  $G_2$  scale according to the mass ratio.

Stellar and gas particles initially have the same particle mass ( $3.3 \times 10^3$  and  $4.6 \times 10^3 M_{\odot}$ , respectively) and softening length (10 and 20 pc, respectively) in all the 10 mergers of the suite. In order to limit excursions of BHs from the centre of each galaxy, we impose the dark matter particles to have a mass smaller than 15 per cent of that of the smaller BH in each merger. For this reason, the mass and softening length of dark matter particles in the 1:1, 1:2, and 1:4 mergers were set to  $1.1 \times 10^5 M_{\odot}$  and 30 pc, respectively. In the other mergers, on the other hand, because of the much lower mass of the secondary BH, dark matter particle masses and softening lengths were lowered accordingly (1:6 merger:  $8 \times 10^4 M_{\odot}$  and 27 pc; 1:10 merger:  $5 \times 10^4 M_{\odot}$  and 23 pc).

Each galaxy is initialized with solar metallicity and a uniform stellar population with an age of 2 Gyr to reflect the young age of the Universe at  $z = 3$ . Without any feedback to heat the gas at the beginning of the simulation, much of the gas initially cools and forms stars. To avoid an unphysical burst of supernovae at the beginning of our merger simulations, we evolve the galaxies in isolation over  $\sim 100$  Myr (relaxation period), during which the SF efficiency is gradually increased, by 50 per cent every  $3 \times 10^4$  yr,

up to the value  $c^* = 0.015$ , in order to obtain galaxies that start the main part of the simulation from the  $z = 3$  sequence of star-forming galaxies (Elbaz et al. 2007) and that obey the Kennicutt–Schmidt relation. Data on SFR are extracted every 1 Myr.

We performed all our simulations using the  $N$ -body SPH code GASOLINE (Wadsley, Stadel & Quinn 2004), an extension of the pure gravity tree code PKDGRAV (Stadel 2001). GASOLINE includes explicit line cooling for atomic hydrogen, helium and metals, as well as a physically motivated prescription for SF, supernova feedback and stellar winds (Stinson et al. 2006). In particular, stars are allowed to form if the parent gas particle is colder than 6000 K and denser than  $100 \text{ cm}^{-3}$ , and supernovae release  $10^{51}$  erg into the surrounding gas, according to the blast wave formalism of Stinson et al. (2006).

### 2.3 Black holes

A recent implementation in the GASOLINE code has been the inclusion of a recipe for BH physics (Bellovary et al. 2010), in which BHs are implemented as sink particles that accrete from nearby gas particles according to an Eddington-limited Bondi–Hoyle–Littleton accretion formula. In order to realistically model accretion from an inhomogeneous mix of hot and cold gas particles around the BH, the accretion rate is computed as the sum of the Bondi accretion rate of each individual gas particle near the BH, including the relative velocity with respect to the BH, rather than simply averaging the gas quantities over all the neighbouring particles. This method allows the accretion rate to be weighted more heavily by nearby, cold, dense gas particles (and less by more distant, hot ones, or particles moving fast with respect to the BH) rather than treating them all equally. Additional information is provided in Capelo et al. (2015).

BH accretion gives rise to feedback, implemented as thermal energy injected into the nearest gas particle according to  $\dot{E} = \epsilon_{\text{f}} \epsilon_{\text{r}} \dot{M}_{\text{BH}} c^2$ , where  $c$  is the speed of light in vacuum,  $\epsilon_{\text{r}} = 0.1$  is the radiative efficiency, and  $\epsilon_{\text{f}}$  is the AGN feedback efficiency, chosen to be equal to 0.001, which is lower than other numerical implementations (see Thacker et al. 2014, for a review) to match the local  $\dot{M}_{\text{BH}} - M_{\text{bulge}}$  relation over the galaxy evolution (see the appendix for a discussion of how the results depend on the feedback strength).

We place a single BH at the centre of each galaxy, after the galaxy has been initialized. Its mass,  $M_{\text{BH}} = 2 \times 10^{-3} M_{\text{bulge}}$ , is set

according to the local  $M_{\text{BH}}-M_{\text{bulge}}$  relation (Marconi & Hunt 2003). The mass of the primary BH ( $BH_1$ ) in each simulation is initially set to  $3.53 \times 10^6 M_{\odot}$ , whereas  $BH_2$  has a mass proportional to the mass ratio between the galaxies, producing a minimum initial mass of  $3.53 \times 10^5 M_{\odot}$  in the 1:10 merger. The softening length of all BHs is set to 5 pc, regardless of their mass. Data on BHAR are extracted every 0.1 Myr. The distance between a BH and the local centre of mass remains small throughout the simulation. The mean distance between the local centre of mass and the BH itself is of the same order as the gravitational softening of the stellar particles, 10 pc.

### 3 GENERAL MERGER BEHAVIOUR

We present the behaviour of one of our mergers in Fig. 1. The reference case is m2.gf0.3.pro, a 1:2 merger, and the differences with other mass ratios, orbital configurations, and gas content are discussed at the end of this section.

We divide each merger into three phases, that we dub ‘stochastic’, ‘merger’ proper, and ‘remnant’. The definition we adopt is based on the behaviour of the specific angular momentum in shells within 1 kpc from the galaxy centre (see Capelo et al. 2015 for details). The stochastic phase lasts until the second pericentric passage, when the galaxies enter in close contact. During this phase, the galaxies behave as they do in isolation. This phase is characterized by a non-evolving specific angular momentum. The merger phase starts at the second pericentre, when the specific angular momentum drops abruptly, because of strong dynamical torques. This phase ends when the specific angular momentum returns to

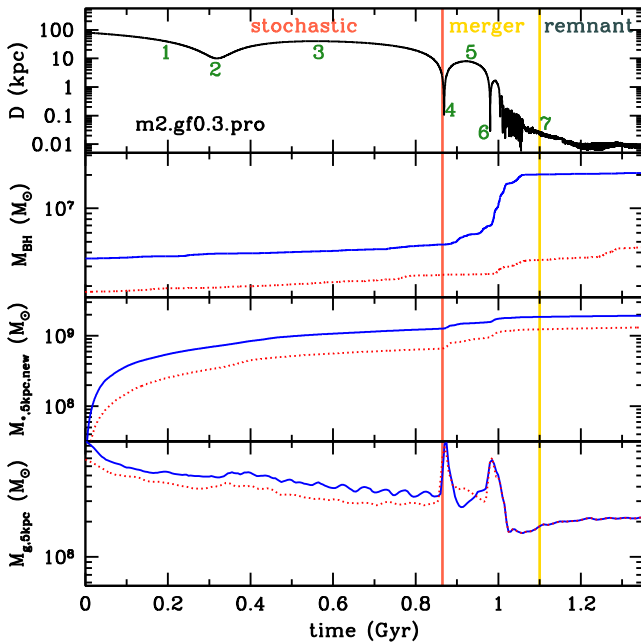


**Figure 1.** Merger properties as a function of time for a 1:2 coplanar, prograde-prograde merger (m2.gf0.3.pro). The entire process is divided into three phases: stochastic, merger, and remnant (see the text for details). First panel: BH separation. Second panel: masses of the two BHs.  $BH_1$  (blue solid line) and  $BH_2$  (red-dotted line). Third panel: cumulative new stellar mass in the central 5 kpc of  $G_1$  (blue solid line) and  $G_2$  (red, dotted line). Fourth panel: gas mass in the central 5 kpc of  $G_1$  (blue, solid line) and  $G_2$  (red-dotted line). The first seven snapshots of the simulation of Fig. 2 are marked in green. The comparison between BH growth and SFR is shown in Fig. 5.

be constant in time, specifically, as the first time after the second pericentric passage when the relative change of specific angular momentum over time increments of 0.05 Gyr is less than 0.3, as in Capelo et al. 2015. The remnant phase lasts from this moment until the end of the simulation. We stop when the remnant phase has reached the same duration as the stochastic phase. Fig. 2 shows snapshots of the galaxies at different times. The three bottom panels of Fig. 1 highlight the differences in the evolution of gas, SF and BH evolution in the three phases.

In the stochastic phase, which, as discussed above, represents also isolated galaxies not involved in mergers, the gas content within 5 kpc steadily decreases because of its consumption by SF. Concurrently, the mass growth of the BHs is smooth and limited, albeit non-zero: the primary BH grows by  $\sim 1.2 \times 10^6 M_{\odot}$  in 0.85 Gyr, and the secondary by  $\sim 6.3 \times 10^5 M_{\odot}$ .

When the merger phase starts, strong gas inflows reach the centres of both galaxies (see Van Wassenhove et al. 2014 and Capelo et al. 2015 for details), enhancing SFR and BHAR. The highest peaks of gas inflows, SFR, and BHAR coincide with the second and third pericentres.

After the merger proper ends, the behaviour in the remnant phase is initially erratic, partly because of feedback effects, and partly because the galaxies are still disturbed. At later times, the conditions return to be similar to what they were in the stochastic phase, although with a somewhat higher BHAR.

Broadly speaking, this behaviour is common to all simulations in our suite. However, as the mass ratio decreases,  $G_1$  becomes more and more insensitive to the dynamical presence of  $G_2$ . Enhancements to BHAR and SFR in the merger phase are noticeable in  $G_1$  for the 1:1, 1:2, and 1:4 mergers, but in the 1:6 and 1:10 mergers they become negligible. Conversely,  $G_2$  is much more strongly affected by the merger dynamics as the mass ratio decreases. Fig. 3 shows the properties of the 1:6 merger, and Fig. 4 illustrates the morphology of the galaxies at different time-steps. In the 1:10 case,  $G_2$  is almost completely disrupted at the third pericentre, and eventually its gas mixes completely with that in the centre of  $G_1$ , becoming fuel for the accretion and growth of  $BH_1$ . In general, we do not see any qualitative difference caused by the orbital inclination, by one of the galaxies being on a retrograde orbit, or by the different gas content.

### 4 TEMPORAL CORRELATION BETWEEN SFR AND BHAR

In this section, we discuss how SFR and BHAR vary temporally with respect to each other. We compare the BHAR to the SFR within shells of 100 pc ( $\text{SFR}_{100\text{pc}}$ ) and 5 kpc ( $\text{SFR}_{5\text{kpc}}$ ) centred around each BH. These shells are our proxies for the nucleus and the entire galaxy.

All merging galaxies calculated in this work qualify as star-forming galaxies at least part of the time during the first two phases. This means that they are on the ‘main sequence’ (or mass sequence; Elbaz et al. 2007; Noeske et al. 2007; Speagle et al. 2014) in the SFR versus stellar mass plane. Discussing the time evolution of the merging galaxies in the SFR versus stellar mass plane is beyond the scope of the present paper. We only use this property when trying to assess (or speculate on) the behaviour of larger merging galaxies that are not included in these calculations, but dominate current observational samples (see discussions in Sections 6 and 7 below).

A delicate issue in this work is the comparison of the merger calculations with observations of samples of star-forming galaxies and AGN. In doing so, we assume that:

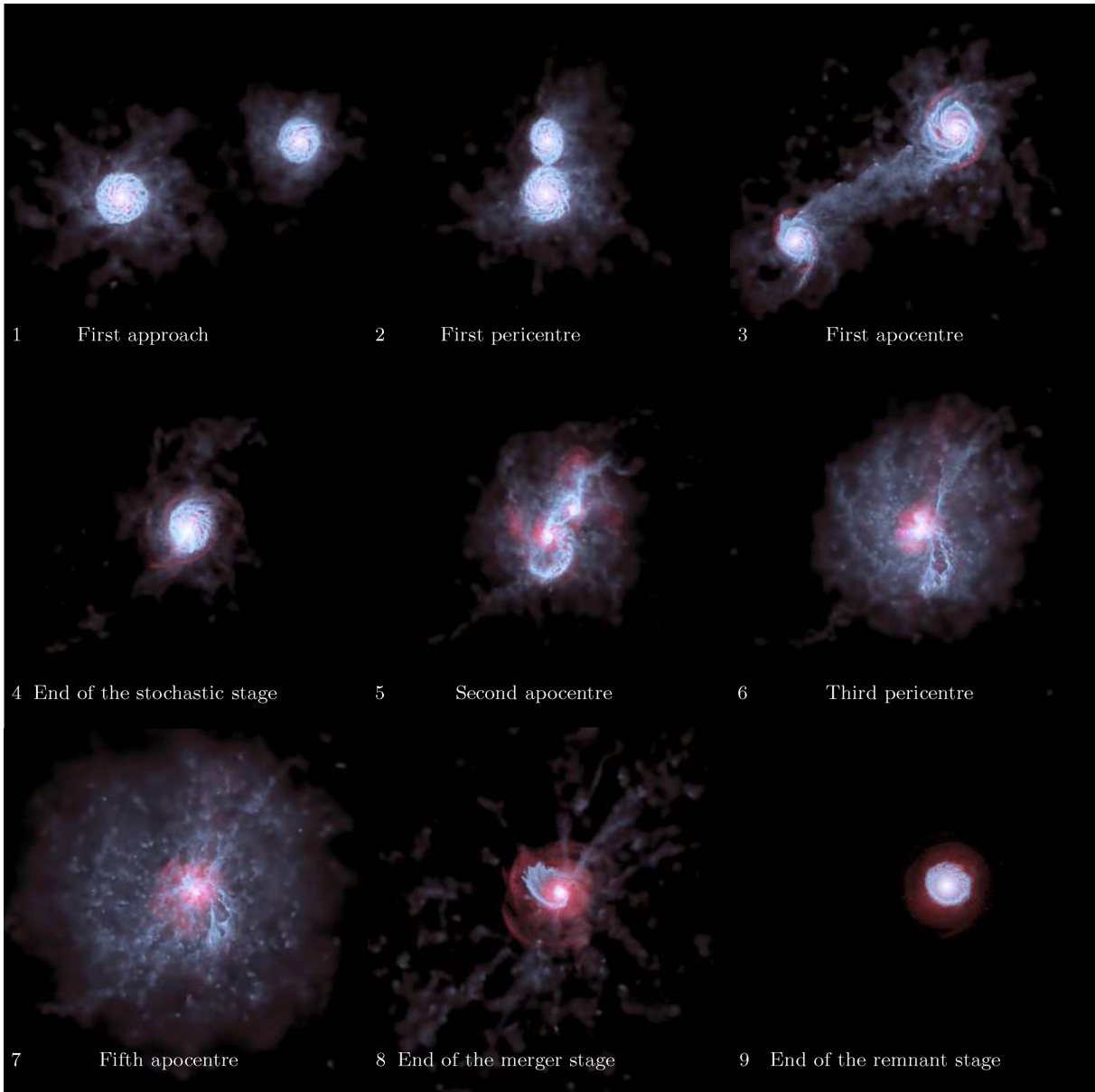


**Figure 2.** Face-on stellar (red) and gas (blue) density snapshots at representative times, in Gyr, of the 1:2 coplanar, prograde–prograde merger: (1) 0.20, (2) 0.32 (first pericentric passage), (3) 0.55 (first apocentric passage), (5) 0.85 (second pericentric passage – end of the stochastic stage), (6) 0.92 (second apocentric passage), (7) 0.98 (fifth apocentric passage), (8) 1.1 (end of the merger stage), (9) 2 (end of the remnant stage), respectively. The image size is  $75 \times 75$  kpc. The gas density is overemphasized with respect to stellar density in order to make the gas more visible.

(i) The collection of all calculations presented here represents a sample of galaxies with masses corresponding to the mass range covered by the calculations.

(ii) The comparison takes into account the relative duration of the three phases. For example, the remnant phase is the longest and, therefore, any comparison with real samples will include many more sources that are in this phase.

(iii) There is a way to extrapolate some of the general properties to larger systems that are not treated in the calculations. This is the most speculative part and we comment of it, more specifically, when addressing the properties in question.

In Fig. 5, we show the evolution of  $\text{SFR}_{100\text{pc}}$ ,  $\text{SFR}_{5\text{kpc}}$ , and BHAR in the reference 1:2 merger, m2.gf0.3.pro, dividing the SFRs by 100 to fit in the same  $y$ -axis range as BHAR. The overall trend of

decreasing global SFR is related to the simulation being evolved in isolation. The differences between phases derived from these simulations can be summarized as follows.

In the first phase, the stochastic phase, BHAR, and nuclear SFR ( $\text{SFR}_{100\text{pc}}$ ) show similar patterns over time-scales of  $\sim 0.05$ – $0.1$  Gyr. We interpret this as caused by being the same gas that feeds the BH and fuels SF. Both BHAR and  $\text{SFR}_{100\text{pc}}$  show also shorter-term variations with large changes, sometime in excess of one order of magnitude over  $0.01$ – $0.1$  Gyr. As a reference, the dynamical time at  $100$  pc is  $0.01$  Gyr. The latter is much less evident in  $\text{SFR}_{5\text{kpc}}$ . SFR in the outer regions is less variable, with changes typically less than a factor of 2. Furthermore, long time-patterns are almost absent. As a reference, the dynamical time at  $5$  kpc is  $\sim 0.2$  Gyr.

In the second, merger phase, the patterns for  $\text{SFR}_{100\text{pc}}$  and BHAR continue to be similar, but now  $\text{SFR}_{5\text{kpc}}$  also exhibits peaks and

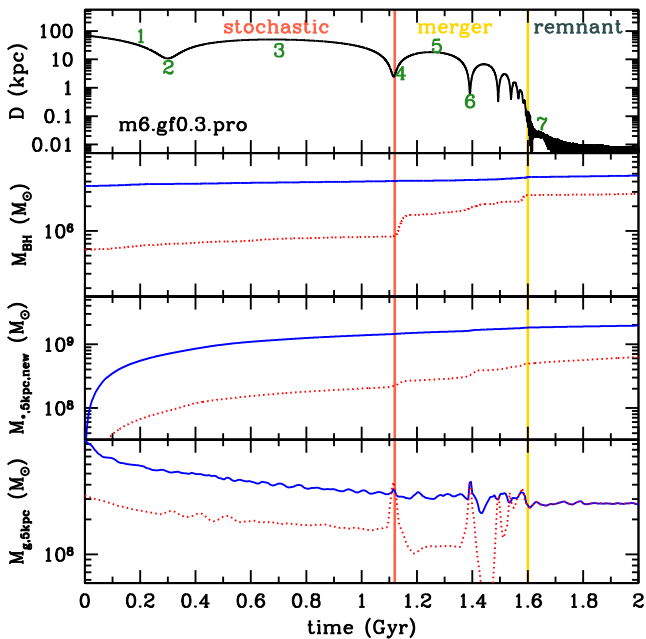


**Figure 3.** As Fig. 1 but for the 1:6 coplanar, prograde–prograde merger (m6.gf0.3.pro). The first seven snapshots of the simulation of Fig. 4 are marked in green. The comparisons between BH growth and SFR are shown in Fig. 7.

troughs over similar time-scales as  $\text{SFR}_{100\text{pc}}$  and BHAR. The fluctuations in  $\text{SFR}_{100\text{pc}}$ ,  $\text{SFR}_{5\text{kpc}}$ , and BHAR increase with respect to the stochastic phase. The peaks in  $\text{SFR}_{5\text{kpc}}$  occur during the second and third pericentres (a small bump can be seen at the time of the first pericentre,  $t = 0.32$  Gyr, in Fig. 5). After the fourth pericentre, the BHs are separated by less than 5 kpc; therefore,  $\text{SFR}_{5\text{kpc}}$  is the same for both BHs.

In the remnant phase, some of the temporal patterns are similar to what they were in the stochastic phase: BHAR and nuclear SFR ( $\text{SFR}_{100\text{pc}}$ ) show similar behaviour, while  $\text{SFR}_{5\text{kpc}}$  does not show specific time-patterns any longer. Note that in the remnant phase the two BHs are separated by a few tens pc at most; therefore,  $\text{SFR}_{5\text{kpc}}$  and  $\text{SFR}_{100\text{pc}}$  are the same for both BHs. In this phase, the two BHs are also enclosed in the same gas density and temperature region, and BHAR is only modulated by the local dynamics, i.e. the relative velocity between each BH and the gas in the Bondi formulation.

To disentangle the time correlation between BHAR and SFR on different scales, we calculated the cross-correlation function of BHAR with  $\text{SFR}_{100\text{pc}}$  and with  $\text{SFR}_{5\text{kpc}}$  (Fig. 6; a positive  $\tau$  means that BHAR lags the SFR). While the general correlation at the peak of the cross-correlation function is not high, it is clear that in all phases BHAR and  $\text{SFR}_{100\text{pc}}$  are better correlated than BHAR and  $\text{SFR}_{5\text{kpc}}$ . The peaks of the BHAR- $\text{SFR}_{100\text{pc}}$  cross-correlation occur close to  $\tau = 0$  Gyr underscoring that they tend to occur simultaneously, and the correlation is strongest during the merger phase. The secondary peaks mark the longer-term patterns visible in Fig. 5 in the stochastic phase, or correlate one pericentre to another during the merger phase. The behaviour in the remnant phase is initially irregular, while at later times the conditions return to be similar to the stochastic phase. The bottom panel shows the autocorrelation functions of BHAR,  $\text{SFR}_{100\text{pc}}$ , and  $\text{SFR}_{5\text{kpc}}$ , highlighting the differences in typical time-scales characteristic of each process and scale. The autocorrelation function is symmetrical around  $\tau = 0$ , where

is always peaks, as the function is identical to itself for no-lag. The presence of additional peaks marks the typical time-scales over which the time-dependent quantity, BHAR,  $\text{SFR}_{100\text{pc}}$ , and  $\text{SFR}_{5\text{kpc}}$  in our case, presents patterns or periodicities. During the stochastic and remnant phase, BHAR and  $\text{SFR}_{100\text{pc}}$  have characteristic time-scales shorter than  $\text{SFR}_{5\text{kpc}}$ , which does not show any peak other than that at  $\tau = 0$ , out to more than 0.3 Gyr. During the merger phase, the intrinsic time-scales are similar for all BHAR,  $\text{SFR}_{100\text{pc}}$ , and  $\text{SFR}_{5\text{kpc}}$ . Recall that the dynamical times are  $\sim 0.01$  Gyr at 100 pc and  $\sim 0.2$  Gyr at 5 kpc, similar to the typical time-scales for SF on these scales.

We can contrast the 1:2 merger used as reference to the 1:6 merger, where the dynamics is very different. As already noted, as the mass ratio decreases,  $G_1$  is less and less affected by the merger. Vice versa,  $G_2$  feels much more strongly the dynamical effects. This is evident in Fig. 7. At second pericentre,  $G_1$  and  $BH_1$  do not experience any burst of SF or BH activity. Instead,  $BH_2$  increases its BHAR (and consequently luminosity) by more than two orders of magnitude. The SFR in  $G_2$  also has a burst affecting the galaxy on all scales (i.e.  $\text{SFR}_{100\text{pc}}$  and  $\text{SFR}_{5\text{kpc}}$ ). During and after the third pericentre,  $\text{SFR}_{5\text{kpc}}$  is enhanced, as  $G_2$  is largely stripped of most of its gas. After  $t = 1.5$  Gyr, the BHs are separated by less than 5 kpc, and hence the green curves in both panels are identical.

From the ensemble of our mergers (see the online-only material), we can identify several common patterns: (i) in the stochastic phase, which applies also to galaxies in isolation,  $\text{SFR}_{5\text{kpc}}$  and BHAR are temporally uncorrelated, while  $\text{SFR}_{100\text{pc}}$  and BHAR show some degree of correlation: the cross-correlation function peaks with a correlation coefficient of  $\sim 0.3$ ; (ii) in the merger phase,  $\text{SFR}_{100\text{pc}}$  and BHAR become more strongly correlated, especially for  $G_2$ ;  $\text{SFR}_{5\text{kpc}}$  and BHAR can have very different behaviours; e.g. be anticorrelated at  $\tau = 0$  in  $G_1$  and positively correlated for  $G_2$  (e.g. m4.gf0.3.pro). (iv) In the remnant phase, the behaviour returns similar to the stochastic phase.

We can only speculate on the expected behaviour in mergers of larger galaxies that we cannot simulate in this work. We expect that the farther the gas is from the centre, the less likely SF will be correlated with BHAR, especially in the stochastic phase when  $\text{SFR}_{5\text{kpc}}$  is completely driven by local dynamics. At pericentre passages, we expect that most of the galaxy will experience a strong perturbation, regardless of its size. Therefore, we expect a weakening of the correlation between  $\text{SFR}_{5\text{kpc}}$  and BHAR during the stochastic phase of larger systems, while  $\text{SFR}_{100\text{pc}}$  and BHAR should behave similarly to the smaller systems treated here.

In summary, SFR and BHAR are both enhanced by the merger dynamics, and how similar temporal behaviour but only for a limited time;  $\sim 0.2$ – $0.3$  Gyr for mass ratios of 1:1 to 1:4. At lower mass ratios, only the smaller galaxy is significantly affected by the dynamics, with bursts of BHAR and SFR in coincidence with pericentric passages, while the larger galaxy is, for the most part, unaware of the merger taking place. A cross-correlation between BHAR and  $\text{SFR}_{100\text{pc}}$  shows some level of correlation even during the stochastic and remnant phases, while BHAR and  $\text{SFR}_{5\text{kpc}}$  are uncorrelated in these two phases. In the merger phase,  $\text{SFR}_{100\text{pc}}$  and BHAR tend to become more correlated, while  $\text{SFR}_{5\text{kpc}}$  and BHAR can be either correlated or anticorrelated at  $\tau = 0$ .

## 5 TIME-VARIABILITY OF SFR AND BHAR

As discussed in the previous section, the cross-correlation function of BHAR and SFR shows some temporal correlation between BHAR and SFR on small scales ( $< 100$  pc) at all times, and

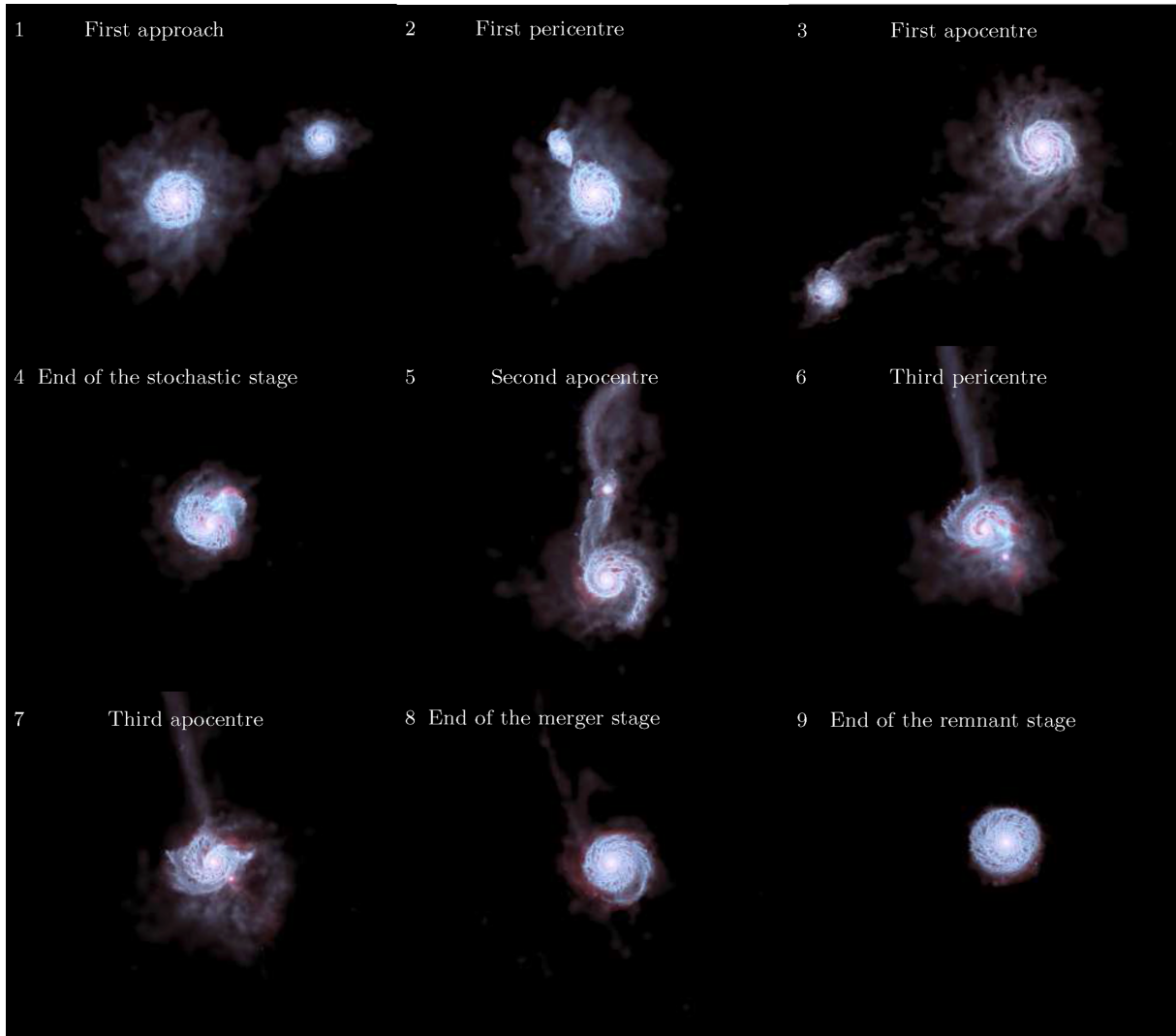


**Figure 4.** Stellar (red) and gas (blue) density snapshots (viewed face-on) at representative times of the 1:6 coplanar, prograde–prograde merger. Times in Gyr are (1) 0.20, (2) 0.30 (first pericentric passage), (3) 0.68 (first apocentric passage), (5) 1.10 (second pericentric passage – end of the stochastic stage), (6) 1.25 (second apocentric passage), (7) 1.40 (third apocentric passage), (8) 1.60 (end of the merger stage), (9) 2.60 (end of the remnant stage). The image size is  $75 \times 75$  kpc. Gas density is overemphasized with respect to stellar density to make it more visible.

between the BHAR and the SFR on larger scales (5 kpc) during the merger phase. Our goal in this section is to test whether the BHAR variability differs between the stochastic and merger phases, what is the connection with the SFR variability, and whether there is a dependence on the scales over which SFR is measured.

As discussed in several recent publications, the different variability time-scales of BHAR and SFR may be responsible for the lack of correlation between SFR and BHAR found in galaxy samples (Aird et al. 2012; Mullaney et al. 2012; Chen et al. 2013; Hickox et al. 2014, see also fig. 9 in Netzer 2009). To extract information on the time-variability of BHAR and SFR, we estimate the time,  $\Delta t$ , needed for each of these quantities to vary by a factor of 10 or a factor of 100. At each time-step, we search forward in time for the first subsequent time-step, within the same phase, where a given quantity (BHAR,  $\text{SFR}_{100\text{pc}}$ , and  $\text{SFR}_{5\text{kpc}}$ ) varies by one of these factors. Note that 1 Myr is the minimum time-scale for SF, i.e. the SF outputs are separated by  $10^6$  years. The distributions we show in Fig. 8 include all the  $\Delta t$  for all the runs. We collect  $BH_1$  and  $BH_2$ , and  $G_1$  and  $G_2$ , for all the simulations listed in Table 1,

as we find no statistical difference if we separate the primary and secondary galaxy and BH.

The  $\Delta t$  distributions show that in the stochastic phase BHAR varies more rapidly than  $\text{SFR}_{5\text{kpc}}$ , and by a larger factor. For instance, we do not see variations in  $\text{SFR}_{5\text{kpc}}$  of a factor of 100 in the stochastic phase, which lasts about 1 Gyr in our runs. BHAR and  $\text{SFR}_{100\text{pc}}$  vary instead over comparable time-scales. In the merger phase, the distributions of  $\text{SFR}_{100\text{pc}}$  and BHAR remain very similar, and  $\text{SFR}_{5\text{kpc}}$  shows higher variability, approaching that of BHAR. When we compare runs with 30 and 60 per cent gas fractions, the only difference we find is that  $\text{SFR}_{100\text{pc}}$  varies more rapidly in the stochastic phase in the high-gas fraction case (the distribution peaks at  $\Delta t = 0.04$  Gyr instead of  $\Delta t = 0.1$  Gyr for the factor of 100 case).

We speculate, again, on what would happen in larger galaxies. In the stochastic phase, the peaks of SFR variability seem to occur over a few dynamical times (1 Gyr corresponds to 5 dynamical times at 5 kpc, and 0.1 Gyr corresponds to 10 dynamical times at 10 kpc); therefore, more massive and extended galaxies would present longer time-variability when considering the galaxy-wide

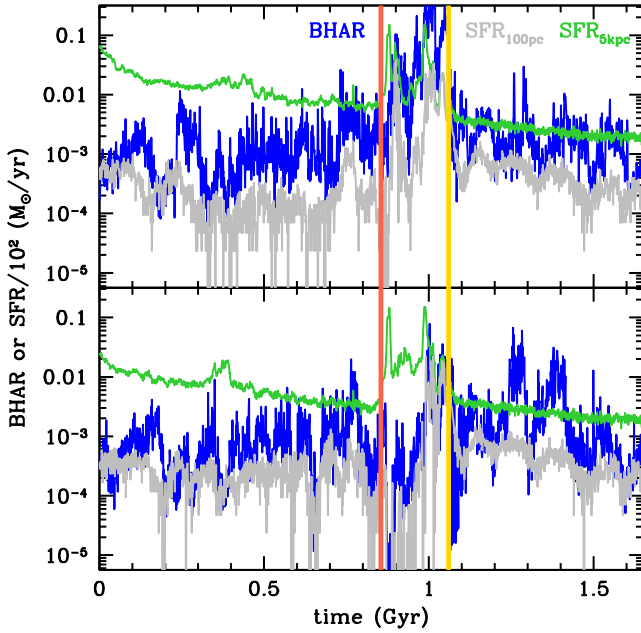


**Figure 5.** BHAR and SFR in the stochastic phase (characterizing also quiescent galaxies in isolation), merger, and remnant phase, for the 1:2 coplanar, prograde–prograde merger (note that the SFR is divided by 100 to fit in the same y-axis range as BHAR). Top panel:  $G_1$ . Bottom panel:  $G_2$ . We show the BHAR (blue, lower thin solid curve), SFR in the central 100 pc (grey, thick solid curve) and SFR inside 5 kpc (green, upper thin solid curve) all as a function of time. The vertical lines mark the transition between the three phases. In the stochastic phase, BHAR and nuclear SFR ( $<100$  pc) show similar trends. The SFR in the outer region is less variable and less correlated with the BHAR compared with the nuclear SFR.

SFR. The nuclear SFR will be instead slower (faster) for galaxies poorer (richer) in gas.

In summary, our simulations, owing to their very high temporal and spatial resolution, confirm the hypothesis that the variability of BHAR is higher than that of SFR measured on large scales (several kpc). However, if the nuclear SFR can be resolved, and SFR measured over short time-scales ( $<100$  Myr), we predict that SFR and BHAR will show similar time-variability.

## 6 RELATIVE GROWTH OF STELLAR AND BH MASS

We now turn to examine the stellar and BH mass growth. For this we use the information in Fig. 9 where we show, explicitly, the ratio of BHAR versus SFR within 5 kpc, for the 1:2 and 1:6 mass ratio mergers, averaging both quantities in bins of 50 Myr (figures for all other simulations are available as online-only material). In the stochastic phase,  $\text{SFR}_{5\text{kpc}}$  is  $\sim 10^3 \times \text{BHAR}$ . If the newly formed stars end up in the bulge, the stochastic phase leads to a scaling between BH mass and bulge mass close to the ‘canonical’ value in the local Universe ( $10^{-3}$ ; Marconi & Hunt 2003; Häring & Rix 2004). This feature, which is common to all our simulations, is not surprising, as we have adjusted the AGN feedback efficiency to agree with the observed BH to bulge mass ratio. Specifically, with a feedback efficiency  $\epsilon_f = 0.001$   $\text{SFR}_{5\text{kpc}}$  is  $\sim 10^3 \times \text{BHAR}$  in the stochastic and remnant phases, and with a feedback efficiency  $\epsilon_f = 0.005$   $\text{SFR}_{5\text{kpc}}$  is  $\sim 10^3 \times \text{BHAR}$  in the merger phase (see the appendix for additional tests of feedback efficiency).

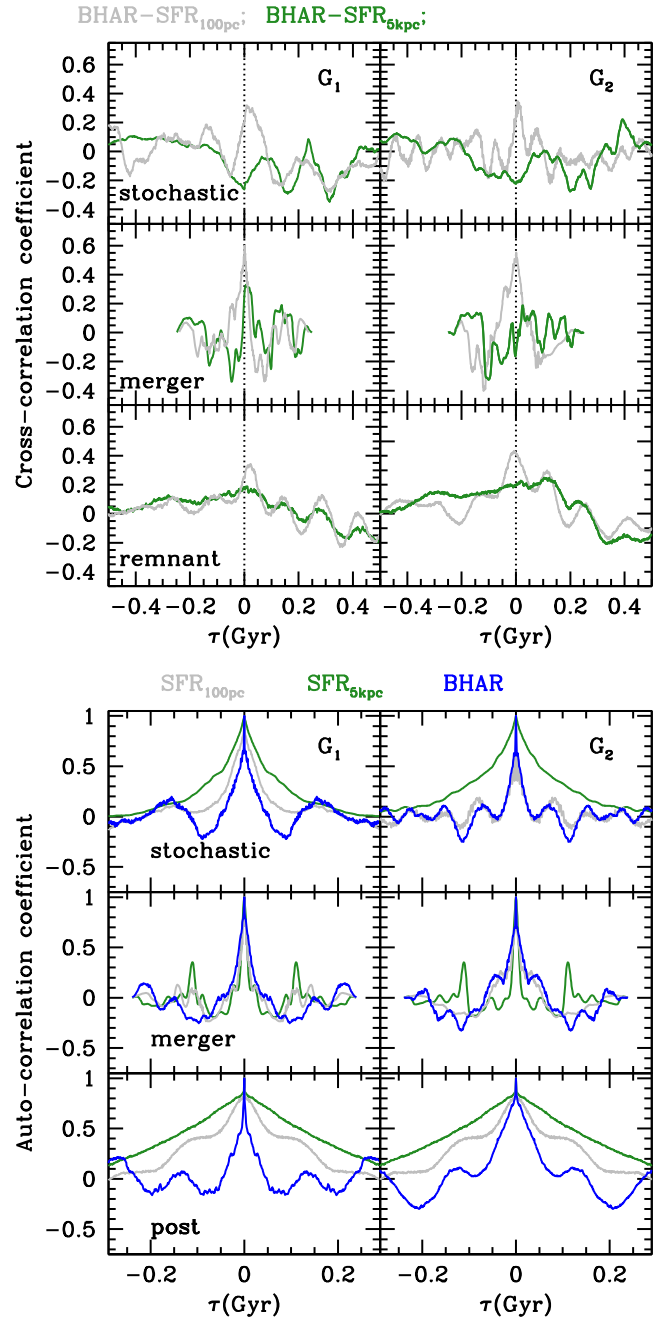


**Figure 6.** Top: cross-correlation coefficient versus time lag,  $\tau$ , for BHAR and SFR, based on the 1:2 coplanar, prograde–prograde merger. Left-hand panel:  $G_1$ . Right-hand panel:  $G_2$ . Some degree of temporal correlation is present between BHAR and  $\text{SFR}_{100\text{pc}}$  at all times. For  $\text{SFR}_{5\text{kpc}}$ , the correlation is much weaker and tends to be present only during the merger proper. Qualitatively, this occurs in many mergers. The behaviour in the remnant phase is initially erratic, and eventually becomes similar to the stochastic stage. Bottom: autocorrelation coefficient versus time lag for BHAR and SFR, based on the 1:2 coplanar, prograde–prograde merger. Left-hand panel:  $G_1$ . Right-hand panel:  $G_2$ . At early and late times, BHAR varies on shorter time-scales than the SFR. During the merger phase, the typical time-scales on all scales are similar.

The merger phase leads, typically, to a higher ratio of BHAR to SFR, and therefore of BH mass to stellar mass. However, there are short episodes where the BHAR drops significantly with respect to the SFR. For instance, for  $BH_2$  at time = 0.87 Gyr in m2.gf0.3.pro

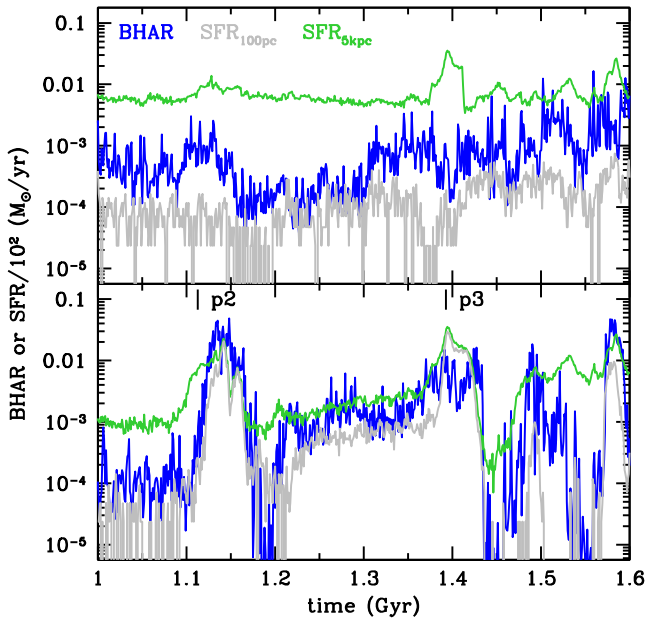


**Figure 7.** BHAR and SFR in the merger phase for the 1:6 coplanar, prograde-prograde merger. Top panel:  $G_1$ . Bottom panel:  $G_2$ . The times of the second and third pericentres are marked as  $p_2$  and  $p_3$ , respectively.

(top panel of Fig. 9). This is caused by a strong burst of SF triggered at the second pericentre, when  $\text{SFR}_{5\text{kpc}}$  increases by a factor of 25. The ensuing supernova feedback depletes the nucleus of gas: the gas mass within the central 100 pc decreases by two orders of magnitude, more than the mass consumed in forming stars within the same time. Once additional gas replenishes the BH environs at the third pericentre, accretion restarts at high levels, with the fiducial ratio between BHAR and SFR, on all scales, of  $\sim \text{few} \times 10^{-3}$ .

While globally the BHAR to SFR ratio is enhanced during the merger phase, periods where the BHAR to SFR ratio is suppressed exist, and they typically follow either bursts in SF or in BH accretion. As noted above, for low-mass ratios (the 1:6 and 1:10 mergers), both  $BH_1$  and  $G_1$  do not ‘notice’ that they are involved in a merger, as the secondary galaxy is only a negligible perturbation.

Since the bulge mass cannot be reliably measured while galaxies are disturbed, we quantify the relative growth of BH and galaxy by estimating the ratio of BH mass to stellar mass within 5 kpc as a function of time (Fig. 10). During the remnant phase, BH accretion remains at levels that are slightly higher than before the merger, keeping the ratio of BH mass to stellar mass roughly constant. At the end of the remnant phase, when the galaxy is relaxed and the bulge mass can be measured, the BH to bulge mass ratio is between 0.0025 and 0.004, i.e. about a factor 1.25–2 higher than in the initial conditions.

A second diagnostic of the enhancement of BHAR relative to the SFR during the merger is the cumulative time fraction spent by the BH and galaxy above a given ratio of BHAR/SFR. This is shown in Fig. 11. For this figure, we combined all our simulations together, and include both  $G_1$  and  $G_2$ , since the difference between the two galaxies is negligible. The horizontal line marks the 50 percent level, and the vertical lines the BHAR/SFR ratio above which the system spends 50 percent of its time. This ratio increases by a factor  $\sim 5$  during the (transitory) merger phase, meaning that during this phase the BH grows more efficiently than its host’s stellar mass, skewing the BH to stellar mass ratio to higher values. We find a very weak dependence of this ratio on orbital configurations, and

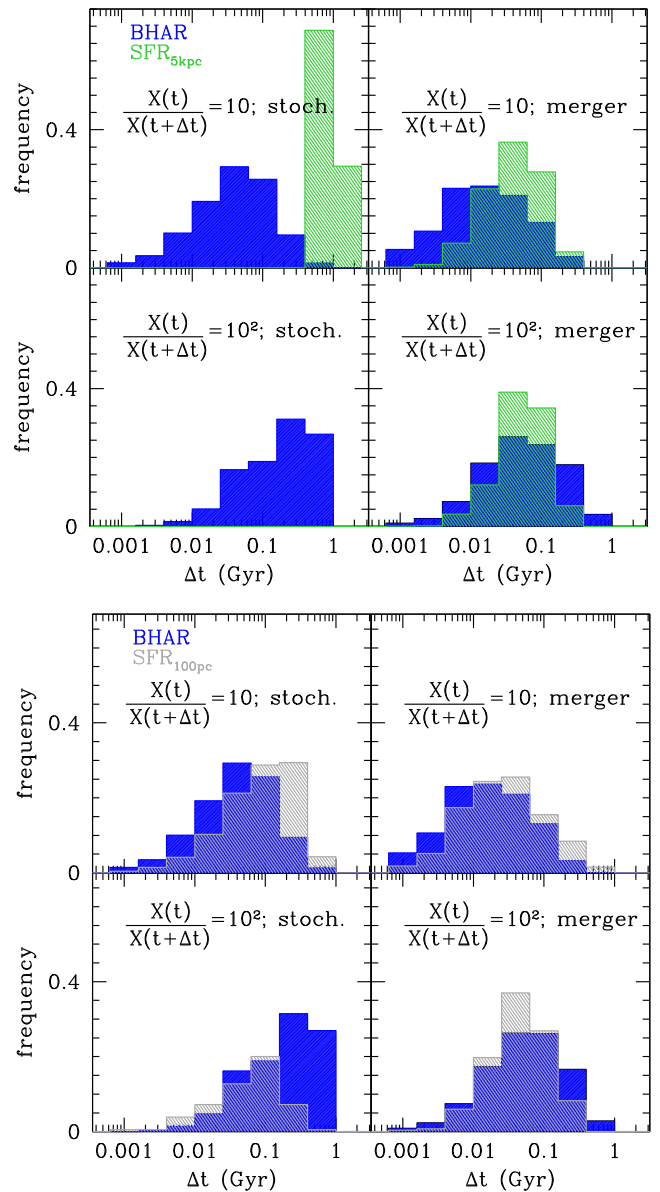


**Figure 8.** Distribution of the time,  $\Delta t$ , needed for a quantity  $X$ , where  $X = \text{BHAR}$  (blue),  $X = \text{SFR}_{100\text{pc}}$  (grey), or  $X = \text{SFR}_{5\text{kpc}}$  (green), to vary by a factor of 10 or 100. In the stochastic phase, the BHAR varies on much shorter time-scales than  $\text{SFR}_{5\text{kpc}}$  and the distinction between the two distributions is clear. In the merger phase, large variations of BHAR and SFR occur over similar time-scales. BHAR and  $\text{SFR}_{100\text{pc}}$  vary over similar time-scales in all cases. The behaviour in the remnant phase (not shown here for clarity) is intermediate between stochastic and merger.

gas fraction, and a somewhat stronger dependence on the mass ratio. For example, the enhancement in the merger phase in the cases of mass ratios 1:6 and 1:10 is completely dominated by  $BH_2$  and  $G_2$ . The appendix gives more details about the dependence on feedback efficiency and resolution.

Regarding more massive galaxies that are included in observational samples, we speculate that their behaviour can be inferred from the present calculations using some well-known properties of star-forming galaxies. In such systems, the stellar mass and SFR are coupled to form the ‘main sequence’, and in general  $\text{SFR} \propto M_*^\alpha$  where  $\alpha \approx 0.7 - 1$  with some hints for changes with redshift. Therefore, for galaxies on the main sequence, SFR would increase

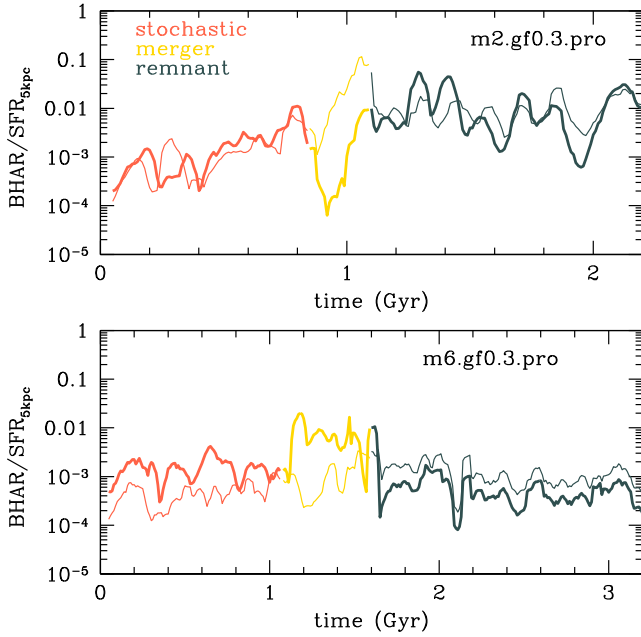


**Figure 9.** Ratio of BHAR to  $SFR_{5kpc}$ , averaging both quantities in bins of 50 Myr for a 1:2 and a 1:6 mass ratio mergers. We distinguish stochastic (red), merger (gold), and remnant (dark grey) phases. Thin curve:  $G_1$ ; thick curve:  $G_2$ . Recall that from half-way through the merger phase, the two BHs are separated by less than 5 kpc, meaning that  $SFR_{5kpc}$  is the same for both BHs. In the minor merger case (mass ratio of 1:6), the larger galaxy is almost unaffected by the merger while the secondary is strongly perturbed.

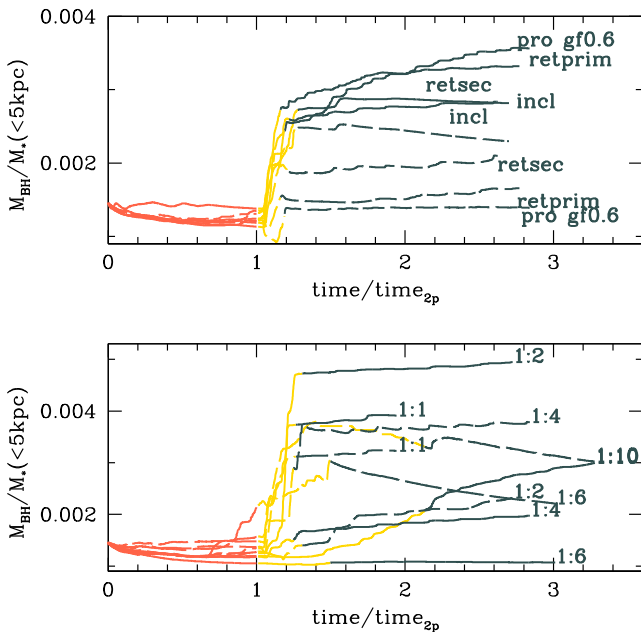


**Figure 10.** Ratio of BH mass to stellar mass within 5 kpc as a function of time, normalized to the time of the second pericentre. Solid curves:  $BH_1$  and  $G_1$ . Dashed curves:  $BH_2$  and  $G_2$ . Top panel: different orbital orientations and gas fractions for the same mass ratio of 1:2. Bottom panel: different mass ratios, from 1:1 to 1:10 for the same coplanar, prograde-prograde orbital configuration. Note how  $G_1$  in the 1:6 merger is almost completely unaffected by the merger. In the remnant phase, it would make more sense to sum the masses of  $BH_1$  and  $BH_2$ , as well as the stellar mass in both galaxies, but this would create a discontinuity in the curves.

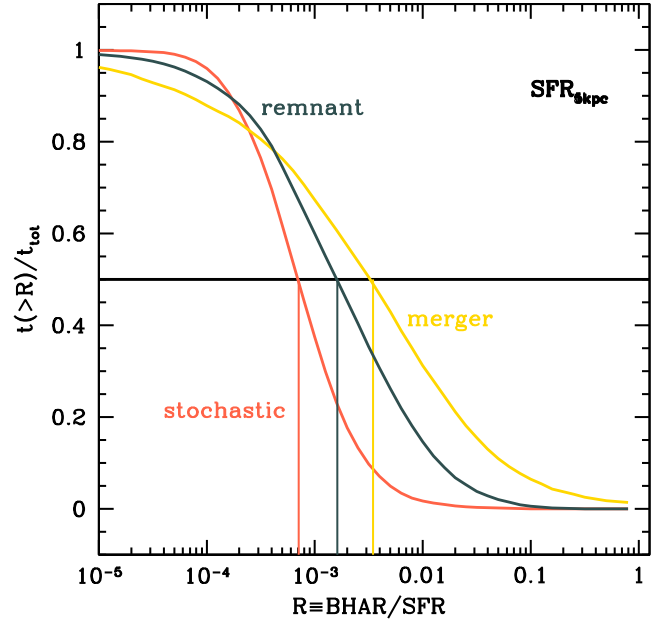


**Figure 11.** Cumulative time fraction above a given ratio of BHAR/SFR within 5 kpc. The numbers apply to all simulations together and include both  $G_1$  and  $G_2$  but we distinguish for each of them the stochastic, merger and remnant phases. The horizontal line marks the 50 per cent level and the vertical lines the BHAR/SFR ratios above which the system spends 50 per cent of its time.

approximately linearly with stellar mass. The galaxies we simulate start on the main sequence, but eventually they move away from it as they consume gas. As a consequence, adopting the linear evolution of SFR with mass characteristic of the main sequence is not rigorously correct at all times, but we can use this approach to infer some trends.

We can conjecture how the BHAR would scale with the galaxy mass taking as a starting point the work by Aird et al. (2012). They find that in a sample of AGN, at  $0.2 < z < 1.0$ , the probability of finding an AGN with a specific accretion rate, i.e. BHAR relative to the stellar mass of the host galaxy, can be described by a power-law distribution, with slope  $-0.65$ , independent of stellar mass (see also Bongiorno et al. 2012, where they find a slope closer to unity). Calculating the same quantity for the collection of all our simulated galaxies (Fig. 12), we find a power law with a slope of  $-0.8$  over three orders of magnitude, in reasonable agreement with Aird et al (2012). Perhaps more important are the slopes of the individual phases. We find that the slope is steeper for the quiescent and remnant phases, and shallower for the merger phase. If the specific accretion rate is self-similar, we expect that in a larger galaxy we would have similar specific accretion rates; therefore, the BHAR would increase linearly with the stellar mass.

Based on these conjectures, therefore, both BHAR and SFR would increase approximately linearly with stellar mass. The results in Figs 9, showing the ratio of BHAR/SFR, and 10, showing the ratio of BH mass to stellar mass, would therefore be in first approximation similar in larger galaxies.

## 7 RELATIVE MAGNITUDE OF SFR AND BHAR

Fig. 13 shows the time evolution of BHAR versus SFR for the reference merger. This figure provides a visual representation of the trajectory of BHAR and  $SFR_{5kpc}$  over time. It complements the

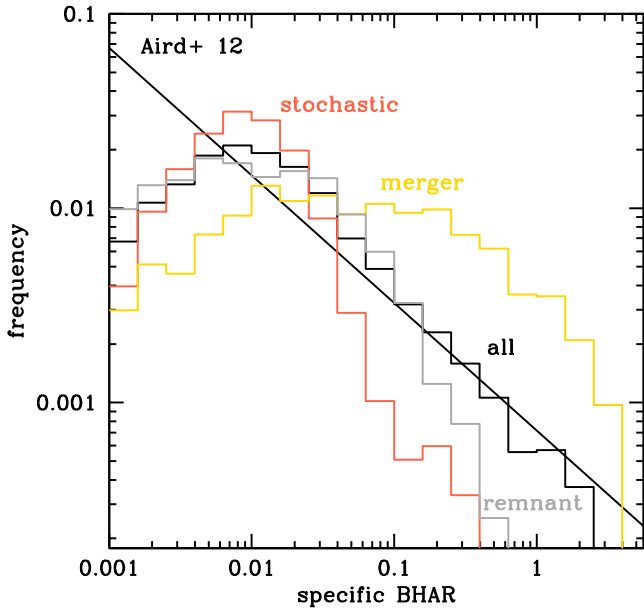


**Figure 12.** Distribution of specific BHAR, i.e. BHAR relative to the stellar mass of the host galaxy, for our simulated galaxies. We distinguish the stochastic (red), merger (gold), and remnant (dark grey) phases. We also combine all phases together (‘all’, black). As a reference, we show the distribution proposed by Aird et al. (2012; solid black line).

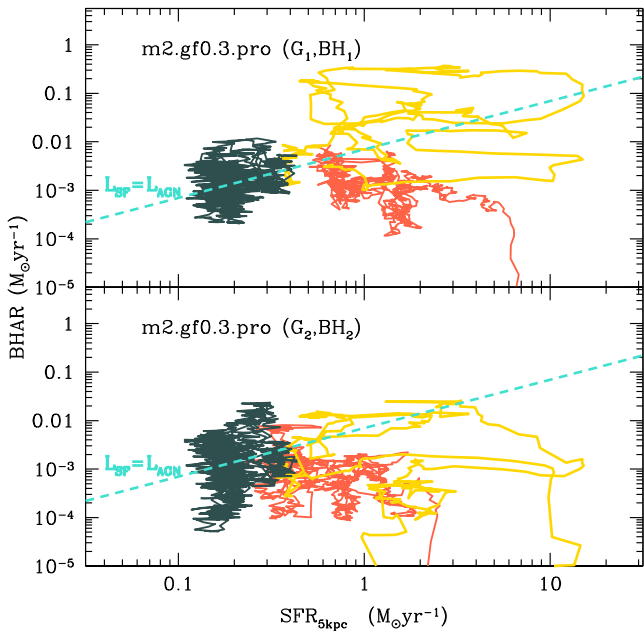


**Figure 13.** Time evolution tracks of BHAR versus SFR for a 1:2 merger with prograde, coplanar configuration and gas fraction 0.3. Individual measurement are spaced by 1 Myr. We distinguish the stochastic (red), merger (gold), and remnant (dark grey) phases. Tracks for all other mergers are available as online-only material.

analysis of Thacker et al. (2014), who present the time evolution of BHAR versus SFR in a series of 1:1 mergers where they vary the BH accretion and AGN feedback. The dashed line marks the boundary of the AGN- versus SF-dominated regions, i.e the regions where  $L_{\text{AGN}}$  is respectively higher or lower than  $L_{\text{SF}}$ . We calculated the AGN luminosity assuming a fixed radiative efficiency  $\epsilon_r = 0.1$ ,

and the far-infrared luminosity by assuming  $10^{10}$  solar luminosities per SFR of one solar mass per year.

In all our simulations, galaxies inhabit the SF-dominated region during the stochastic phase and move between the AGN- and the SF-dominated regions during the remnant phase. However, during the merger phase, the evolution is complex and chaotic (see tracks for all simulations in the online-only material). In general, not all mergers lead to an appreciable enhancement of AGN activity and not all mergers lead to an appreciable enhancement of SF. For instance, the bottom panel of Fig. 13 is a clear example of a case where BH accretion is not enhanced.

We can translate the BHAR-SFR tracks into a different representation by averaging SFR and BHAR in all simulations over the same time span, e.g. 10 Myr (Fig. 14, left-hand panels). BHAR and  $\text{SFR}_{100\text{pc}}$  show some degree of correlation, although the scatter is large (2 dex in BHAR at fixed  $\text{SFR}_{100\text{pc}}$ ). If we were able to measure the BHAR and the SFR that occurred within the same time span, we would find that BHAR and  $\text{SFR}_{100\text{pc}}$  correlate for both quiescent and merging hosts. BHAR and  $\text{SFR}_{5\text{kpc}}$ , instead, do not correlate.

So far we have addressed the question of whether a correlation between SFR and BHAR exists a priori. In the following, we discuss our results taking the observers’ view and asking whether a correlation between SFR and BHAR can be inferred from the observations, by considering the different time-scales probed by measurements of the AGN luminosity and SFR. Most SFR diagnostics measure the ongoing, rather than instantaneous SFR. To mimic this, we average the SFR at each time-step over the previous 100 Myr. BHAR is averaged instead over 1 Myr time-steps. Only a random subsample of the points in each phase matching the number of points in the left-hand panels is shown, to avoid the figure being overcrowded. We bundled all our simulations together, but we distinguished for each of them the stochastic (red), merger (gold), and remnant (dark grey) phases. Fig. 14, right-hand panels, shows the results of this analysis. To guide the eye, we include curves from observational studies focusing on AGN (Rosario et al. 2012) or galaxies (Mullaney et al. 2012; Chen et al. 2013). We postpone the detailed comparison with observations to a forthcoming dedicated paper.

In the stochastic phase, the time-scale over which SFR is estimated has a limited effect, as the SFR varies over relatively long time-scales (cf. Fig. 8) and the magnitude of the changes in SFR and BHAR is small. The main effect is in removing the low- and high-SFR peaks, and as a consequence slightly tilting the BHAR- $\text{SFR}_{5\text{kpc}}$  distribution. In the merger phase, several effects should be taken into account. In the first few 100 Myr of the merger phase, the average SFR includes part of the stochastic phase. Since in this phase the SFR is better correlated with the BHAR, the averaging washes out this underlying correlation. This is particularly evident for  $\text{SFR}_{100\text{pc}}$  (bottom panel of Fig. 14). A very similar average SFR is associated with a wide range of BHAR, as during the merger phase both BHAR and SFR vary by a large factor over short time-scales (cf. Fig. 8). The main effect can be seen at the high-SFR end of the BHAR- $\text{SFR}_{100\text{pc}}$  distribution, as the average  $\text{SFR}_{100\text{pc}}$  in the merger phase is high, while the instantaneous BHAR varies by several orders of magnitude. The remnant phase is different again. Here there is no difference between measuring the ongoing or the instantaneous SFR, except in the first few 100 Myr that include part of the merger phase. In summary, for merging and post-merger galaxies, a time-averaged SFR worsens the BHAR- $\text{SFR}_{100\text{pc}}$  correlation, without affecting much the behaviour of BHAR versus  $\text{SFR}_{5\text{kpc}}$ .

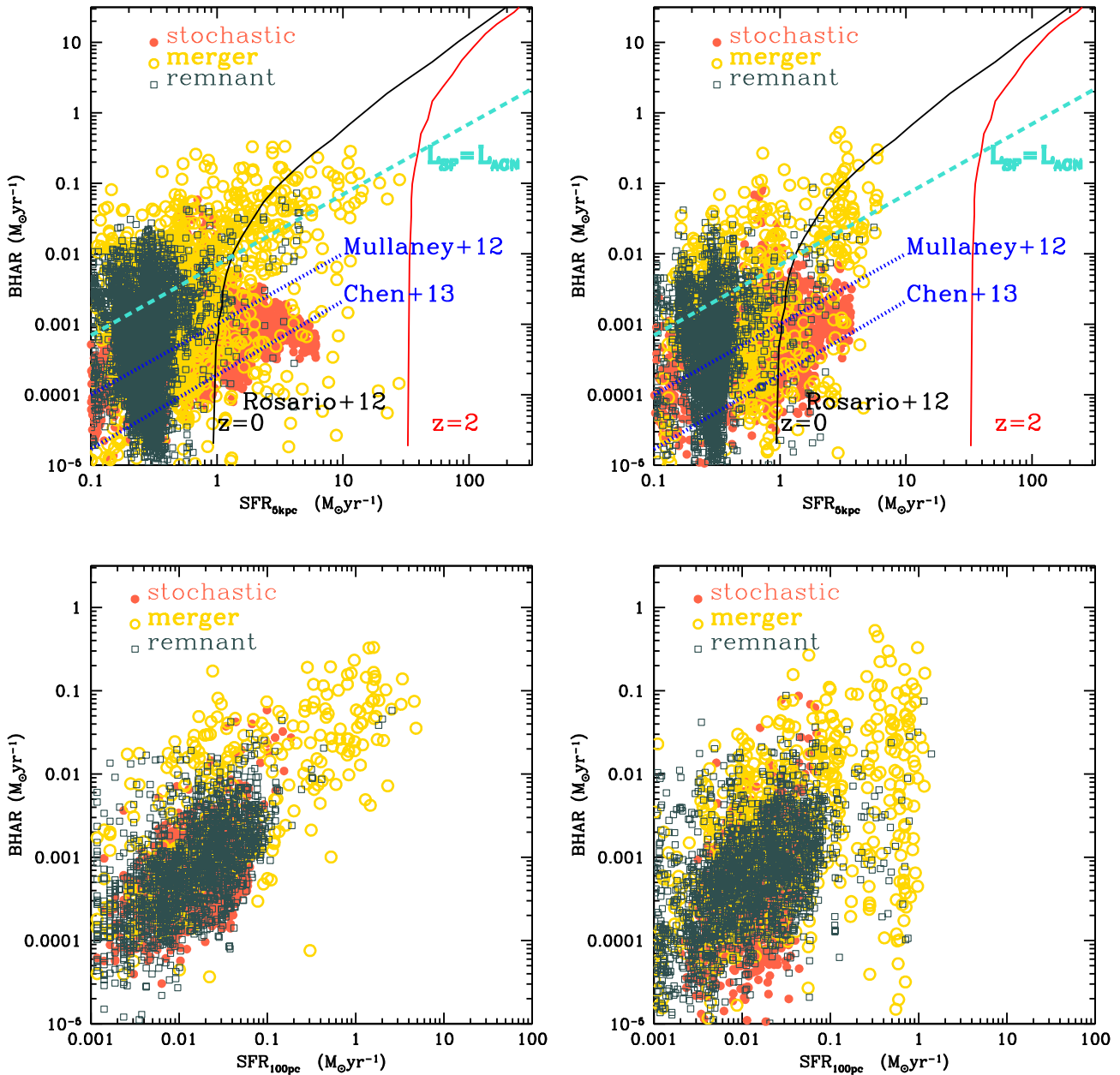


**Figure 14.** BHAR versus SFR within 5 kpc (top), and within 100 pc (bottom). In the two left-hand panels, we average both quantities in bins of 10 Myr. In the two right-hand panels, we average the SFR over the last 100 Myr before the time-step used for the BHAR calculation, to mimic observational SFR indicators. In the top panels, we include curves from Rosario et al. (2012; AGN, red and black), and from Chen et al. (2013; star-forming galaxies, blue). We also mark the AGN- and SF-dominated regions, respectively, above and below the light blue line.

## 8 CONCLUSIONS

We present a suite of simulations devoted to the detailed study of BH and galaxy properties during various type mergers. This is the first suite that reaches consistent high time (data on BHAR are extracted every 0.1 Myr, and data on SFR are extracted every 1 Myr), mass ( $3.3 \times 10^3$  and  $4.6 \times 10^3 M_{\odot}$ , for stars and gas, respectively) and spatial (10 and 20 pc, for stars and gas, respectively) resolution for a range of mass ratios that includes minor mergers, down to 1:6 and 1:10. We set the initial pericentre distance near 20 per cent of the virial radius of  $G_1$ , and start from a separation equal to the sum of the virial radii of the two galaxies, in order to be consistent with cosmological orbits. We run the simulation for a time which

is long enough to include the return of the final remnant phase to a quiescent state. This allows us to capture the post-merger phase, which may represent the state where most AGN are observed, as they show no hint of a companion galaxy. The set-up allows us to resolve nuclear gas inflows in the innermost region ( $< 100$  pc) where BHAR takes place, as well as to resolve the SF within the galaxy. We can also meaningfully compare BHAR and SFR time-scales, both in an abstract way (i.e. instantaneous SFR and BHAR occurring within the same time-step) and in a realistic way more appropriate for a comparison with the observations (ongoing SFR). We analyse the three phases that we dub ‘stochastic’ (corresponding to a galaxy in isolation or in the early phases of an encounter), ‘merger’ proper (when the merger dynamics dominates), and ‘remnant’ (from the

end of the merger to the return to quiescence). Our findings can be summarized as follows:

(i) The temporal patterns of BHAR and  $SFR_{5\text{kpc}}$  are generally uncorrelated, except in some cases during the strongest pericentre passages.  $SFR_{100\text{pc}}$  and BHAR show some level of correlation during all the stochastic, merger, and remnant phases.

(ii) For galaxies in quiescence or post-merger, BHAR varies more rapidly than  $SFR_{5\text{kpc}}$ , but on time-scales similar to  $SFR_{100\text{pc}}$ . For AGN in the merger phase, BHAR and SFR are expected to show similar time-variability even on galactic scales.

(iii) The merger phase leads, in most cases, to a higher BHAR/SFR, by a factor of a few, when averaged over time, and therefore to high BH mass to stellar mass. However, there are short episodes when BHAR drops with respect to the SFR, because of supernova and AGN feedback triggered by a previous burst of SF or BH activity.

(iv) When measured over the same time-scales, BHAR and  $SFR_{100\text{pc}}$  are proportional to each other. The correlation lessens if the ongoing rather than the instantaneous SFR is measured, since the average SFR is associated with a wide range of BHAR.

(v) The time-scale over which SFR is measured affects less strongly the interpretation of BHAR versus  $SFR_{5\text{kpc}}$ . BHAR and  $SFR_{5\text{kpc}}$  show different behaviour during the three stages. From a rough proportionality in the stochastic phase, with  $BHAR \sim 10^{-3} SFR_{5\text{kpc}}$  (and a large scatter), to  $BHAR \sim 10^{-2} SFR_{5\text{kpc}}$  for the most luminous AGN in the merger phase. In the remnant phase, galaxies occupy a region where a limited range in  $SFR_{5\text{kpc}}$  corresponds to a large range of BHARs.

A major conclusion of our study is that any comparison between BH activity and SFR must take into account the different stages of the merger process since those properties can change dramatically. While in the stochastic phase galaxies would, for the most part, not be considered AGN, the merger phase is when AGN and SF activity is close to their peak. The remnant phase is characterized by a large range of BHARs, moving, at times, the galaxy into the AGN-dominated region. An AGN can be caught sometime (up to 1.5 Gyr) after the merger and starburst actually took place. Study of BH activity and SFR in large AGN and galaxy samples must take into account the different durations of the various phases. Finally, we have shown that SFR diagnostics that provide a measure of the recent, rather than present one, affect the recovery of the underlying population properties.

## ACKNOWLEDGEMENTS

MV thanks D. Alexander, E. Daddi and V. Wild for valuable suggestions and discussions. MV acknowledges funding support from NASA, through award ATP NNX10AC84G, from SAO, through award TM1-12007X, from NSF, through award AST 1107675, and from a Marie Curie FP7-Reintegration-Grant within the 7th European Community Framework Programme (PCIG10-GA-2011-303609). HN acknowledges support by the Israel Science Foundation grant 284/13 This work was granted access to the HPC resources of TGCC under the allocations 2013-t2013046955 and 2014-x2014046955 made by GENCI. This research was supported in part by the National Science Foundation under grant no. NSF PHY11-25915, through the Kavli Institute for Theoretical Physics and its program ‘A Universe of Black Holes’. PRC thanks the Institut d’Astrophysique de Paris for hosting him during his visits.

## REFERENCES

- Adelberger K. L., Steidel C. C., Pettini M., Shapley A. E., Reddy N. A., Erb D. K., 2005, *ApJ*, 619, 697
- Aird J. et al., 2012, *ApJ*, 746, 90
- Alexander D. M., Hickox R. C., 2012, *New Astron. Rev.*, 56, 93
- Bellovary J. M., Governato F., Quinn T. R., Wadsley J., Shen S., Volonteri M., 2010, *ApJ*, 721, L148
- Bellovary J., Brooks A., Volonteri M., Governato F., Quinn T., Wadsley J., 2013, *ApJ*, 779, 136
- Benson A. J., 2005, *MNRAS*, 358, 551
- Blecha L., Cox T. J., Loeb A., Hernquist L., 2011, *MNRAS*, 412, 2154
- Bongiorno A. et al., 2012, *MNRAS*, 427, 3103
- Callegari S., Mayer L., Kazantzidis S., Colpi M., Governato F., Quinn T., Wadsley J., 2009, *ApJ*, 696, L89
- Callegari S., Kazantzidis S., Mayer L., Colpi M., Bellovary J. M., Quinn T., Wadsley J., 2011, *ApJ*, 729, 85
- Capelo P. R., Volonteri M., Dotti M., Bellovary J. M., Mayer L., Governato F., 2015, *MNRAS*, 447, 2123
- Chen C.-T. J. et al., 2013, *ApJ*, 773, 3
- Di Matteo T., Springel V., Hernquist L., 2005, *Nature*, 433, 604
- Diamond-Stanic A. M., Rieke G. H., 2012, *ApJ*, 746, 168
- Elbaz D. et al., 2007, *A&A*, 468, 33
- Ferrarese L., Merritt D., 2000, *ApJ*, 539, L9
- Gabor J. M., Bournaud F., 2013, *MNRAS*, 434, 606
- Gültekin K. et al., 2009, *ApJ*, 698, 198
- Häring N., Rix H.-W., 2004, *ApJ*, 604, L89
- Hayward C. C., Torrey P., Springel V., Hernquist L., Vogelsberger M., 2014, *MNRAS*, 442, 1992
- Heckman T. M., Kauffmann G., Brinchmann J., Charlot S., Tremonti C., White S. D. M., 2004, *ApJ*, 613, 109
- Hernquist L., 1990, *ApJ*, 356, 359
- Hickox R. C., Mullaney J. R., Alexander D. M., Chen C.-T. J., Civano F. M., Goulding A. D., Hainline K. N., 2014, *ApJ*, 782, 9
- Hopkins P. F., Hernquist L., Cox T. J., Di Matteo T., Robertson B., Springel V., 2006, *ApJS*, 163, 1
- Johansson P. H., Naab T., Burkert A., 2009, *ApJ*, 690, 802
- Kauffmann G., Haehnelt M., 2000, *MNRAS*, 311, 576
- Khochfar S., Burkert A., 2006, *A&A*, 445, 403
- Kormendy J., Ho L. C., 2013, *ARA&A*, 51, 511
- Lutz D. et al., 2008, *ApJ*, 684, 853
- Magorrian J. et al., 1998, *AJ*, 115, 2285
- Marconi A., Hunt L. K., 2003, *ApJ*, 589, L21
- Merloni A., Rudnick G., Di Matteo T., 2004, *MNRAS*, 354, L37
- Mullaney J. R. et al., 2012, *ApJ*, 753, L30
- Navarro J. F., Frenk C. S., White S. D. M., 1997, *ApJ*, 490, 493
- Neistein E., Netzer H., 2014, *MNRAS*, 437, 3373
- Netzer H., 2009, *MNRAS*, 399, 1907
- Netzer H. et al., 2007, *ApJ*, 666, 806
- Noeske K. G. et al., 2007, *ApJ*, 660, L47
- Rosario D. J. et al., 2012, *A&A*, 545, A45
- Silk J., 2013, *ApJ*, 772, 112
- Silverman J. D. et al., 2008, *ApJ*, 679, 118
- Silverman J. D. et al., 2009, *ApJ*, 696, 396
- Speagle J. S., Steinhardt C. L., Capak P. L., Silverman J. D., 2014, *ApJS*, 214, 15
- Springel V., White S. D. M., 1999, *MNRAS*, 307, 162
- Springel V., Di Matteo T., Hernquist L., 2005, *ApJ*, 620, L79
- Stadel J. G., 2001, PhD thesis, Univ. Washington
- Stinson G., Seth A., Katz N., Wadsley J., Governato F., Quinn T., 2006, *MNRAS*, 373, 1074
- Thacker R. J., MacMackin C., Wurster J., Hobbs A., 2014, *MNRAS*, 443, 1125
- Van Wassenhove S., Volonteri M., Mayer L., Dotti M., Bellovary J., Callegari S., 2012, *ApJ*, 748, L7
- Van Wassenhove S., Capelo P. R., Volonteri M., Dotti M., Bellovary J. M., Mayer L., Governato F., 2014, *MNRAS*, 439, 474

Wadsley J. W., Stadel J., Quinn T., 2004, *New Astron.*, 9, 137  
 Wild V., Kauffmann G., Heckman T., Charlot S., Lemson G., Brinchmann J., Reichard T., Pasquali A., 2007, *MNRAS*, 381, 543  
 Wild V., Heckman T., Charlot S., 2010, *MNRAS*, 405, 933

## APPENDIX A: PARAMETER STUDY: RESOLUTION AND FEEDBACK EFFICIENCY

In this section, we discuss the robustness of our results against resolution and AGN feedback efficiency (see also Thacker et al. 2014). We have performed three lower-resolution simulations of the 1:2 coplanar, prograde–prograde merger with 30 per cent gas fraction (m2.gf0.3.pro), where we degraded the mass resolution by a factor of 4, and the softening by a factor  $4^{1/3}$ , one with the same feedback efficiency of  $\epsilon_f = 0.001$  as in the high-resolution suite, one with  $\epsilon_f = 0.002$  and one with  $\epsilon_f = 0.005$ . We have also performed an additional high-resolution simulation with  $\epsilon_f = 0.005$ .

In Fig. A1, we compare the BHAR and SFR for these four runs of the same merger (‘lr’ and ‘hr’ in the figure captions stands for low-resolution and high-resolution respectively), excluding the nuclear SFR,  $\text{SFR}_{100\text{pc}}$ , as we do not resolve adequately that region in the low-resolution runs. We supplement this figure with the SFR within 1 kpc as a proxy for the central regions, however. It is clear that  $\text{SFR}_{5\text{kpc}}$  is robust against changes in resolution or AGN feedback efficiency during the stochastic phase, while the BHAR decreases as AGN feedback strength increases. In the merger phase, local dynamics becomes more important than feedback efficiency for BHAR, and the low-resolution run with  $\epsilon_f = 0.001$  has a BHAR similar to the low-resolution runs with  $\epsilon_f = 0.002$  and  $\epsilon_f = 0.005$ . The new stellar mass formed changes by at most 30 per cent among runs with different  $\epsilon_f$ . On the other hand, resolution has an important effect: small-scale gravitational torques and small-scale overdensities cannot be resolved at low-resolution, leading to an ‘average’ BH growth that may be higher than (e.g. in the case of  $BH_1$ ) or similar to (in the case of  $BH_2$ ) the high-resolution run, where the region near the BHs is well resolved (see Fig. A2,  $0.85 < t < 1.1$  Gyr). The stellar mass formed changes by up to 50 per cent in runs with different resolution.

In general, different AGN feedback strength or resolution modify the normalization of the SFR or BHAR, but not their temporal trends (Fig. A3). Therefore, the results discussed in Sections 3 and 4 are robust against the choice of parameters and resolution, keeping in mind the caveat that  $\text{SFR}_{100\text{pc}}$  cannot be measured for the low-resolution runs as the 100 pc region is not sufficiently resolved. We also find that the results on variability presented in Section 5 are also robust: the time over which SFR and BHAR vary is not much affected by the AGN feedback efficiency or resolution.

The results discussed in Sections 6 and 7 are more sensitive to changes in the normalization of SFR and BHAR, and we warn the reader to keep this caveat in mind. In particular, in all but the low resolution,  $\epsilon_f = 0.001$  run, we see consistently an increase in the ratio between BHAR and SFR in the merger phase compared to the stochastic phase. In the low resolution,  $\epsilon_f = 0.001$  run shown in Fig. A2 the stellar growth is the largest, while the BH growth is limited. If we take the ratio of BH mass to stellar mass, in the stochastic phase, this ratio tends to decrease, and the decrease is stronger the higher is  $\epsilon_f$ . Therefore, this trend is caused primarily by the effect of AGN feedback on the BHAR (SFR is almost unaffected as discussed above). The ratio shows a high-value plateau during the merger phase for all mergers, and returns to roughly constant or decreasing values.

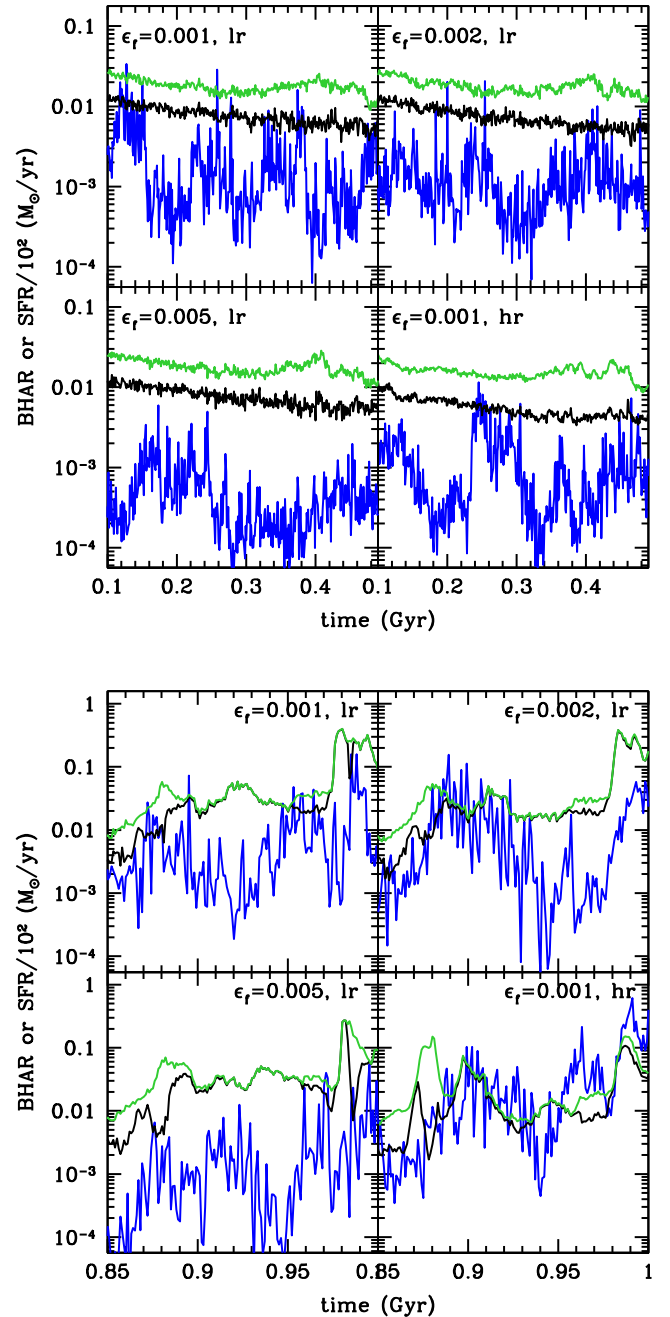


**Figure A1.** Effect of changing resolution (lower resolution by a factor of 4) and feedback efficiency ( $\epsilon_f = 0.002$  or  $0.005$ ) for  $G_1$  in the 1:2 coplanar, prograde–prograde merger with a gas fraction of 30 per cent. Feedback efficiency and resolution are labelled in each panel. For each simulation, we select the same time-steps (top four panels: stochastic phase; bottom four panels: merger phase). We show the BHAR (blue, lower thin solid curve) and the SFR in the central 1 kpc (black, thick solid curve) and 5 kpc (green, upper thin solid curve) all as a function of time.

Fig. A4 explicitly shows how the ratio BHAR/SFR within 5 kpc, averaging both quantities in bins of 50 Myr, depends on resolution and feedback efficiency. By increasing the feedback efficiency, the BHAR is affected more than  $\text{SFR}_{5\text{kpc}}$ , i.e. the ratio decreases as  $\epsilon_f$  increases. As a consequence, in the run with  $\epsilon_f = 0.005$ , longer time is spent at a lower ratio between BHAR and  $\text{SFR}_{5\text{kpc}}$ : 50 per cent of

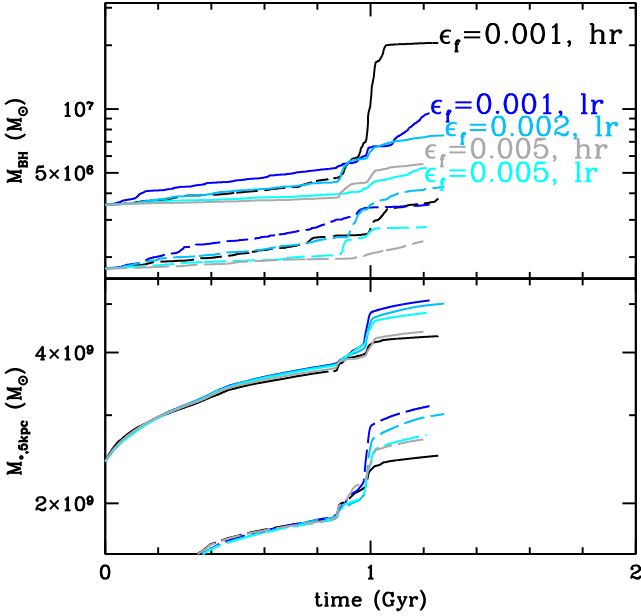


**Figure A2.** Effect of changing resolution (lower resolution by a factor of 4) and feedback efficiency ( $\epsilon_f = 0.002$  or  $0.005$ ) on the BH (top,  $BH_1$ : solid;  $BH_2$ : dashed) and stellar growth (bottom,  $G_1$ : solid;  $G_2$ : dashed) in the 1:2 coplanar, prograde–prograde merger with gas fraction 30 per cent. The colour coding is labelled for  $BH_1$  and applies to all curves.

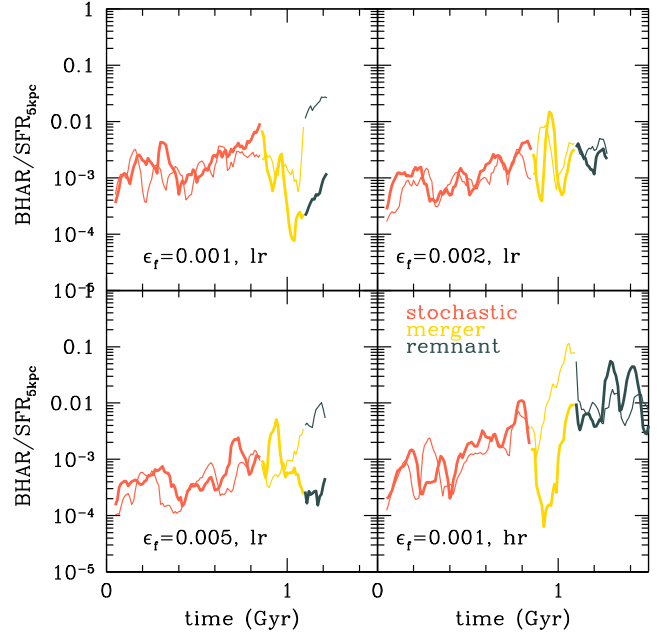


**Figure A4.** Ratio of BHAR versus SFR within 5 kpc, averaging both quantities in bins of 10 Myr illustrating the effect of changing resolution (lower resolution by a factor of 4) and feedback efficiency ( $\epsilon_f = 0.002$  or  $0.005$ ).

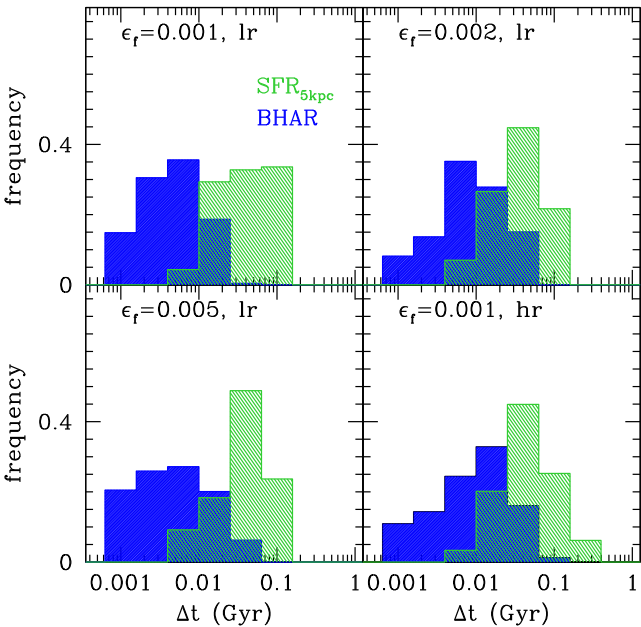


**Figure A3.** Distribution of the time,  $\Delta t$ , needed for a quantity  $X$ , where  $X = \text{BHAR}$  (blue) and  $X = \text{SFR}_{5\text{kpc}}$  (green), to vary by a factor of 10 during the merger phase. The results on temporal variability are robust against different resolution or feedback efficiency choices.

the time in the stochastic phase is spent at a ratio  $< 2 \times 10^{-4}$ , and 50 per cent of the merger phase has ratio  $< 10^{-3}$ . We nevertheless find a relative enhancement between the stochastic and merger phase. We note that if AGN feedback were as strong as  $\epsilon_f = 0.005$  BHs would require growth boosts driven by mergers

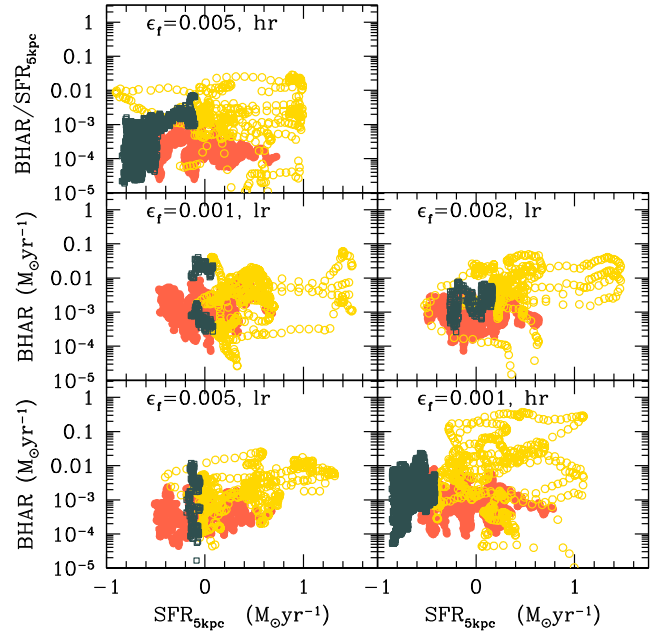


**Figure A5.** BHAR versus SFR within 5 kpc (top) and within 100 pc (bottom), averaging both quantities in bins of 10 Myr illustrating the effect of changing resolution (lower resolution by a factor of 4) and feedback efficiency ( $\epsilon_f = 0.002$  or  $0.005$ ).

in order to attain, over cosmic history, a mass compatible with the BH–bulge correlation. The feedback strength we chose for the reference runs allows the BHs to grow towards the BH–bulge correlation through stochastic low-level activity, rather than through merger-driven events (Bellovary et al. 2013).

Finally, if we plot BHAR versus  $\text{SFR}_{5\text{kpc}}$  (Fig. A5; cf. Fig. 14), we find consistent trends regardless of resolution and AGN feedback efficiency. In the stochastic phase, we obtain a roughly spherical blob spanning the same BHAR and SFR as in Fig. 14 (red–orange points), while in the merger phase the blob expands to higher BHAR and SFR, as in the reference run (golden points). Low-resolution runs show, visually, a somewhat better SFR–BHAR trend for all feedback efficiencies.

## SUPPORTING INFORMATION

Additional Supporting Information may be found in the online version of this article:

**Part1.pdf**

**Part2.pdf**

**Part3.pdf** (<http://mnras.oxfordjournals.org/lookup/suppl/doi:10.1093/mnras/stv387/-/DC1>).

Please note: Oxford University Press are not responsible for the content or functionality of any supporting materials supplied by the authors. Any queries (other than missing material) should be directed to the corresponding author for the article.

This paper has been typeset from a  $\text{\TeX}/\text{\LaTeX}$  file prepared by the author.